Geophys. J. R. astr. Soc. (1984) **79**, 987–1022 and *Microfiche* GJ 79/1

Tectonic evolution of the North Sea basin: crustal stretching and subsidence

Penny Barton and Rosy Wood* *Bullard Laboratories, Madingley Rise, Madingley Road, Cambridge CB3 0EZ*

Received 1984 June 22; in original form 1983 December 19

Summary. The lithospheric stretching model for the formation of sedimentary basins was tested in the central North Sea by a combined study of crustal thinning and basement subsidence patterns. A profile of crustal structure was obtained by shooting a long-range seismic experiment across the Central Graben, the main axis of subsidence. A seabed array of 12 seismometers in the graben was used to record shots fired in a line 530 km long across the basin. The data collected during the experiment were interpreted by modelling synthetic seismograms from a laterally varying structure, and the final model showed substantial crustal thinning beneath the graben. Subsidence data from 19 exploration wells were analysed to obtain subsidence patterns in the central North Sea since Jurassic times. Changes in water depth were quantified using foraminiferal assemblages where possible, and observed basement subsidence paths were corrected for sediment loading, compaction and changes in water depth through time. The seismic model is shown to be compatible with the observed gravity field, and the small size of observed gravity anomalies is used to argue that the basin is in local isostatic equilibrium. Both crustal thinning and basement subsidence studies indicate about 70 km of stretching across the Central Graben during the mid-Jurassic to early Cretaceous extensional event. This extension appears to have occurred over crust already slightly thinned beneath the graben, and the seismic data suggest that total extension since the early Permian may have been more than 100 km. The data presented here may all be explained using a simple model of uniform extension of the lithosphere.

1 Introduction

1.1 MODELS OF SEDIMENTARY BASIN FORMATION

The phenomenon of long-term vertical movement of the crust, occurring far from a plate boundary, is a puzzling feature of the continents. Long-term downward movement of a region creates a sedimentary basin. Bally (1982) defines a sedimentary basin as 'a region

*Now at British Petroleum, Britannic House, Moor Lane, London EC2Y 9BU.

that has subsided, that contains sediment in excess of 1 km, and that is today still preserved in a more or less coherent form'. Many models for the formation of sedimentary basins have been proposed, but most are difficult to test. We examine one particular basin, believed representative of a type, in the light of a simple quantitative model of basin formation by stretching the lithosphere.

Sedimentary basins may be divided into two types (Beaumont, Keen & Boutilier 1982):

(1) Those dominated by compressional tectonics which cause flexural loading of the lithosphere.

(2) Those located in aseismic regions in isostatic equilibrium.

This investigation is restricted to the second, passive type, and in particular the North Sea basin.

The formation of passive basins has been predicted as the outcome of stretching of the lithosphere (McKenzie 1978). We have tested the stretching model in the North Sea using two independent lines of evidence. We present a profile of the crust perpendicular to the Central Graben and subsidence data for nearby exploration wells. The amount of lithospheric stretching suggested by crustal thinning beneath the Graben is compared with that implied by the subsidence history recorded in the wells, and a tentative history of the basin's formation is proposed.

Passive basins have a number of features which must be explained by any model for their formation. The subsidence history, preserved in the thick sediments, consists of rapid initial subsidence accompanied by faulting, followed by slow sinking which, when the loading effect of the sediment is removed, follows an exponential decay with time similar to that observed in the oceans (Sleep 1971). There is no evidence for major uplift or vulcanism, and the thick sediments are not accompanied by a significant gravity anomaly. The subsidence patterns observed in sedimentary basins are similar to those of passive continental margins, such as the North American Atlantic margin (Royden & Keen 1980; Steckler & Watts 1981).

A simple model of extension of the lithosphere (McKenzie 1978) predicts the formation of sedimentary basins and of passive margins by the same mechanism, shown in Fig. 1. The lithosphere (Fig. 1a) responds to a period of rapid stretching by faulting in the brittle upper crust and necking in the ductile lower crust and mantle (Fig. 1b). The hot asthenosphere rises passively into the space above, distorting the isotherms. Continued extension results in failure of the continental lithosphere and the formation of a new ocean basin. If stretching stops, the initial subsidence by faulting is followed by a steady thermal subsidence as the upwelled asthenosphere contracts and sinks, cooling back to an equilibrium thermal gradient.

Various adaptions of the simple model have been suggested, including subcrustal erosion (Ziegler 1982b), intrusion of dyke swarms into the crust (Royden, Sclater & Von Hertzen 1980) or asthenospheric melt into the base of the crust (Keen, Beaumont & Boutilier 1981), different amounts of stretching in the upper and lower lithosphere (Royden & Keen 1980), and lateral flow in the ductile lower lithosphere (Bott 1976). However, it is difficult to test for complexities of this sort, and they need not be considered unless they are required to account for observations not predicted by the simpler model.

A model which has predictive properties, particularly if they are quantitative, may be tested by experiment, and may also be used as an interpretive framework for observations. First, the stretching model may be used to predict subsidence paths for the sediment column in a basin formed by a stretching event of given rate and duration (Jarvis & McKenzie 1980). The theoretical paths may be compared with data from exploration wells in order to estimate the implied amount of extension.

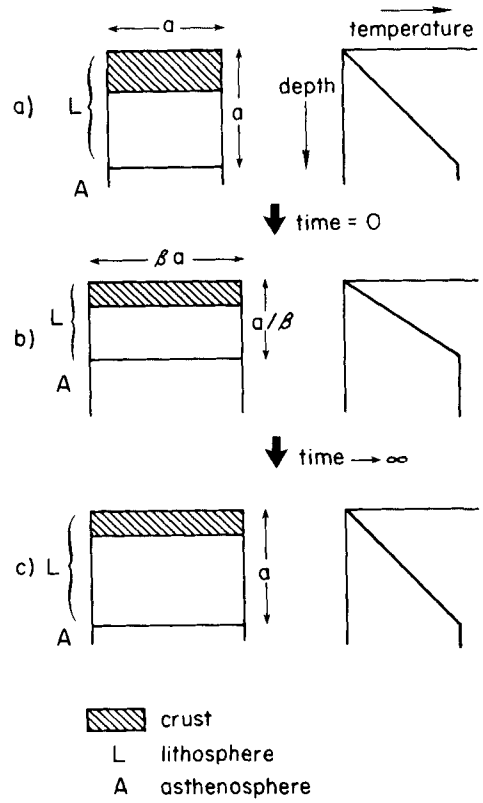

Figure 1. Stretching–subsidence model for the formation of sedimentary basins after McKenzie (1978). During extension rapid isostatic subsidence takes place by active faulting. Subsequently, isotherms distorted during the initial extension return slowly to equilibrium causing contraction of the cooling asthenosphere and regional subsidence. The stretching factor, β, is defined as the increase in surface area due to extension.

Secondly, assuming that crust is conserved, the simplest prediction of the model is that a stretched region will retain an anomalously thin pre-subsidence crust, even after the decay of thermal effects (Fig. 1c). A direct measurement of the crustal thickness allows a test of the model which is independent of studies of the sediment outlined above.

Thirdly, the model specifies the temperature structure of the sediments through time, a relationship which is used widely to predict reactions between organic substances involved in the maturation of hydrocarbons (Mackenzie & McKenzie 1983).

Lastly, it should be possible to estimate the amount of crustal stretching by measurement of extension of basement faults. In practice this is a difficult problem. Fault patterns are complex and three-dimensional, and there is little consensus amongst such estimates of extension due to various interpretations of fault geometry (Ziegler 1982b, 1983; Foucher, Le Pichon & Sibuet 1982; Montadert *et al.* 1979; Le Pichon & Sibuet 1981; Bally 1982). Additionally, current theories of fault evolution (Proffett 1977; Jackson & McKenzie 1983) suggest that visible high-angle faults may represent only the most recent generation of faulting in a region; older faults have rotated to near horizontal and are difficult to detect. Some estimates of stretching based on commercial seismic reflection data from the North Sea have been significantly lower than the amount estimated from crustal thickness or subsidence data (Ziegler 1983; L. Davidson private communication), an observation which has led to suggestions of an additional agent thinning the crust (Ziegler 1982b, 1983).

However, recent work on SALT2, a deep seismic reflection line acquired by BIRPS exactly coincident with the refraction experiment discussed here, shows that a wide range of stretching factors, embracing those implied by the crustal thickness/subsidence studies in this paper, may be inferred from the faults visible on the reflection data (W.S.Q. Allerton private communication). We are aware that significant discrepancies between stretching estimates from fault reconstructions and from crustal thickness/subsidence studies would necessitate modification of the simple stretching model discussed here. However, the combination of interpretational difficulties discussed above, together with continual improvements of basement imaging and hence a constant increase in the number of faults detected, lead us to conclude that these discrepancies do not demonstrably exist (Barton & Wood 1983).

1.2 THE NORTH SEA BASIN

The sediments of the North Sea basin are thoroughly explored and well documented (Ziegler 1982a, b; Woodland 1975; Illing & Hobson 1981), and only a brief outline is necessary here.

Little is known of the geology of the pre-Devonian basement, except where it is sampled in about 30 wells (Frost, Fitch & Miller 1981). Ar/Ar and K/Ar dating of the rocks, medium to high grade metamorphics, indicate that they were deformed during the Caledonian orogeny (410–450 Myr ago). The Midland Valley of Scotland subsided rapidly during the Devonian and Carboniferous, acting as a centre of sedimentation in the western North Sea. During the Permian two basins formed separated by the mid-North Sea–Ringkobing Fyn High. In both basins several kilometres of salt were deposited. The northern Permian basin was centred about 80 km to the east of the subsequent Tertiary basin. The Variscan deformation front did not extend into the North Sea area (Frost *et al.* 1981).

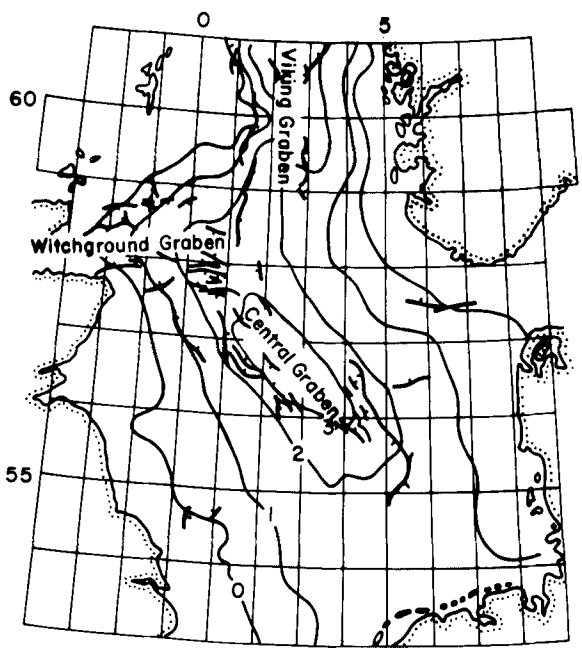

Figure 2. Map of North Sea sedimentary basin, showing main graben faults (tick on downthrown side) and Tertiary isopachs in kilometres. Note the symmetrical saucer-shaped Tertiary basin centred over the Central Graben.

The Triassic saw the initiation of the three-armed graben system which dominates the structure of the present-day basin (Fig. 2). Thick sediments almost completely filled the grabens by the end of the Triassic. Further rifting during the middle and late Jurassic continued into the early Cretaceous, with movement of the Permian salt initiated by faulting (Taylor 1981). Since the Danian there has been continuous subsidence and infill of the basin with fine-grained sediments, interrupted only by the minor Laramide (Early Palaeocene) tectonic episode. Tertiary sediments reach thicknesses of over 3 km in the Central Graben area.

The subsidence history of sediments from wells in the Witchground Graben (Christie & Sclater 1980; Wood 1981) and the Central Graben (Sclater & Christie 1980) has been compared with theoretical subsidence curves calculated from the stretching model. The subsidence data of Sclater & Christie (1980) is compatible with stretching factors of 1.5–2.0 in the centre of the basin, whereas Wood's (1981) more detailed study of the Witchground Graben implies a slightly lower stretching factor for the mid-Jurassic extensional event. Sclater & Christie (1980) compare subsidence data with theoretical curves obtained assuming instantaneous extension, and do not allow for variations in water depth through time when unloading the basement.

A number of long-range seismic refraction lines have been used to measure crustal thickness and structure in the North Sea. In the southern North Sea, Collette *et al.* (1970) found a Moho depth of about 31 km. Further north, lines have been shot across the Viking Graben (Solli 1976; Sørnes 1971) and the Witchground Graben (Christie 1982), and thinning of the crust is observed beneath both grabens (Ziegler 1978; Christie & Sclater 1980). Both profiles may be criticized for poor control on lower crustal velocities used in the conversion to depth of Moho time-terms. The major centre of sediment deposition is the Central Graben (Fig. 2), which is thus the axis of predicted maximum thinning. Prior to the experiment described here, no deep refraction line existed across, or east of, the Central Graben.

We will first discuss the seismic evidence for thinned crust beneath the Central Graben of the North Sea (Section 2). A short section on gravity interpretation (Section 3) shows that the seismic model is compatible with gravity observations, and that the compensation of the sedimentary load is isostatic. The subsidence history of 19 exploration wells in the central North Sea is analysed in Section 4, followed in Section 5 by comparison of results from the two methods and discussion of their implications for the tectonic history of the North Sea basin.

2 Seismic experiment

A long-range seismic refraction experiment, designed to give a crustal profile beneath the Central Graben, was shot from the *RRS John Murray* during the summers of 1981 and 1982. Data were collected using 12 Pull-Up Shallow-water Seismometers (PUSSes) (Smith & Christie 1977) deployed as a linear array in the Central Graben. Sixteen shots of GEOPHEX, ranging in size from 75 kg to 1 tonne, were fired along a line between Edinburgh and Southern Norway at ranges up to 300 km in either direction (Fig. 3). The 'F' shots re-occupied sites of previously determined Moho time-terms (Christie 1979) and the intention of the experiment was to use these shots to get time-terms beneath the PUSS array, and thence beneath shots east of the Graben. The permanent receiver networks at NORSAR, LOWNET, Eskdalemuir and Dublin also recorded the shots, and temporary land arrays were laid out in the Southern Uplands of Scotland, by Edinburgh University, and in southern Norway, for the piggyback experiment CANOBE (Cassell *et al.* 1983). The present analysis is confined to the data collected with the sea-bottom array.

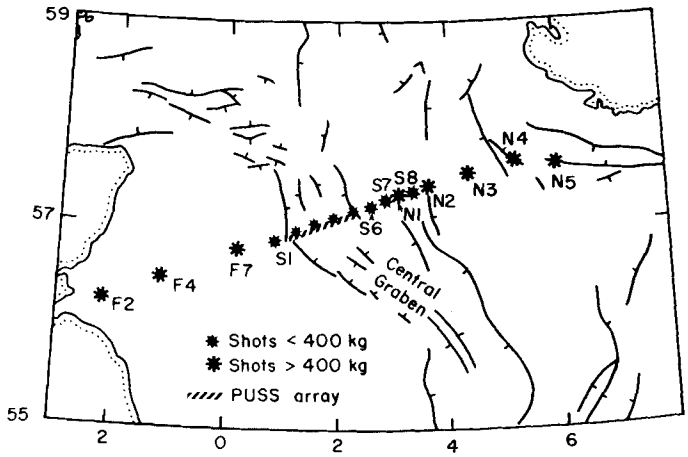

Figure 3. Map of refraction experiment across the Central Graben of the North Sea. Stars mark shot-points, large stars show shots larger than 400 kg. 'F' shots are fired on sites where time-terms to the Moho were pre-determined by Christie (1979). 'N' shots were also recorded on the mainland of Norway during the CANOBE experiment (Cassell *et al.* 1983). Slashed line shows position of array of 12 PUSSes, spaced approximately every 5 km along this line. Graben faults schematic.

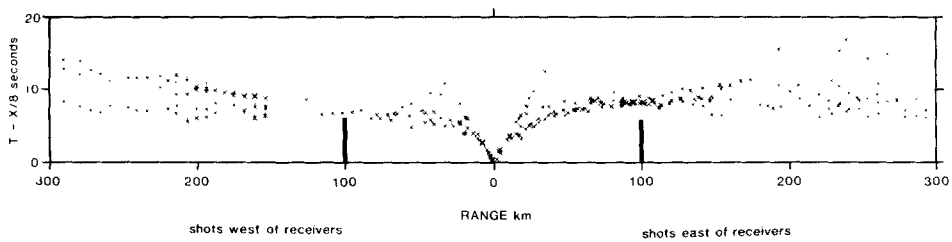

Figure 4. Travel-time plot of arrival picks from seismograms, reduced at 8.0 km s^{-1}. Energy travelling from west to east is plotted on the left side of zero distance; east to west on the right side. Estimated uncertainties in time marked by vertical bars within crosses average uncertainty approximately 0.1 s. Note wide scatter around travel-time branch, and lack of distinct refractors. Identical vertical bars at 100 km range show the asymmetry between the two sides of the plot.

Analogue records from the instruments were digitized, and a composite record section of seismograms from all shots and receivers was plotted. Energy travelling west–east (shots west of the receiver array) was plotted separately from that travelling east–west. Arrival picks from this record section are shown in Fig. 4 and are listed on microfiche accompanying this issue. This plot has three important features:

(1) The arrivals do not lie on discrete branches past ranges of about 30 km.

(2) There is a scatter of about 2 s (20 times the average uncertainty in picking) about the first arrival curve.

(3) There is a significant difference in travel times to similar ranges between west and east sides (see vertical bars on Fig. 4).

These feature suggest that the crustal structure beneath was heterogeneous and unlayered, with a marked asymmetry between west and east sides of the Graben. Due to the disordered nature of the composite record section, the seismograms for each shot are plotted separately and appended on *Microfiche* GJ 79/1.

An initial analysis of the data was carried out using time-term solutions. A set of time-terms to the Moho was obtained for 23 stations across the North Sea, constrained at both ends by independently determined values from Christie (1979) and Cassell *et al.*'s (1983) model. Conversion from time-terms to depth was carried out using evidence from other refraction surveys in the area, and constrained to be consistent with minimal gravity anomalies.

By 1981 the use of time-terms for the analysis of refraction data from laterally varying structures had been superseded by computer modelling techniques. The time-term-derived depth structure of the North Sea crust was used as a starting model for modelling both amplitude and travel-time information for all the data using a newly-developed program for the calculation of synthetic seismograms in laterally varying media.

RAYSYN, a program developed by Cassell (1982), sets up a 2-D crustal model as an array of small square boxes each containing constant seismic parameters, and interfaces consisting of connected linear segments. Thus a ray travelling through the model meets only plane interfaces, which makes computation simple and rapid. Continuous variation of seismic parameters is simulated provided large numbers of boxes are used to specify the model.

Seismograms were difficult to interpret except in the context of the arrival of energy from a single shot across the receiver array. The 12 long-range shots (F2, F4, F7, S1, S6, S7, N1, S8, N2, N3, N4 and N5) were each recorded by up to 12 seismometers. Recordings at the same range at the same or opposite sides of the Central Graben have different travel times and amplitudes, and the phases have different apparent velocities and distribution on the record section. Significant features (beginnings and ends of phases, apparent velocities, relative amplitudes) were identified on each set of observed seismograms. A seismic model was gradually developed which would simulate all of these features in the synthetic seismograms. This model was further constrained to be consistent with the observed gravity field in the area (see Section 3).

2.1 SEDIMENTS

The basement of the North Sea was viewed through a sediment blanket as thick as the oceanic crust and much more inhomogeneous. Sediments in the North Sea reach thicknesses of over 7 km in the Central Graben, and account for about 2.5 s of one-way travel time. Isolation of travel-time contributions from the crystalline crust from those in superficial layers requires detailed knowledge of this upper structure.

Fortunately, it was not necessary to model the sedimentary basin using records from the experiment. A sediment cross-section beneath the refraction line (Fig. 5) was compiled based on Shell depth and velocity data (P. Ziegler private communication) and the North Sea Regional Seismic maps published by the British Geological Survey (Day *et al.* 1981). The profile was checked against isopach maps for the Zechstein (Taylor 1981) and information from the Norwegian Petroleum Directorate (S. Mykkeltveit private communication) and the BGS (D. Smythe private communication).

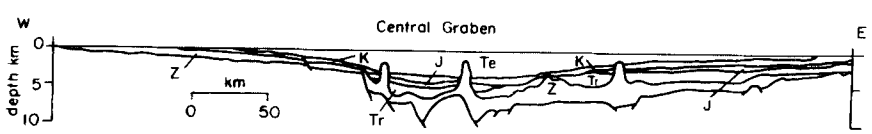

Figure 5. Geological section beneath the refraction profile after P. Ziegler (private communication) and Day *et al.* (1981). Te, Tertiary; K, Upper Cretaceous; J, Lower Cretaceous and Jurassic; Tr, Triassic; Z, Zechstein. Vertical exaggeration 5 : 1.

Modelling was run with two scales of boxes: a large-scale model of the whole line with 1 km-square boxes, and a small-scale model of the Central Graben area, where the experiment gave short range information, with 250 m-square boxes. In each case the total number of boxes, and hence the dimension of each box, is limited by the storage capacity of the computer. The 250 m-square box size allowed the main sedimentary horizons to be represented separately. The seismograms to be modelled using the full crustal model (1 km-square boxes) consist of arrivals which follow a near vertical path through the sediments. Thus the sediment column was represented at this large scale by a layer of the correct thickness and average vertical velocity of the sediments. Horizontal velocity variation accounted for facies changes across the basin.

Even the small-scale model required considerable simplification of the sediment section and basement topography. Features such as fault blocks and salt domes, which undoubtedly affect the records in both travel time and amplitude, could not be represented. The effects of such features on the seismograms were evaluated using idealized models of a small area with high box density.

2.1.1 Fault blocks

The aspect ratio, depth of burial, separation, throw and orientation of a 'typical' North Sea basement fault block were quantified. A simple model consists of flat sedimentary layers underlain by a basement regularly faulted with such blocks (Fig. 6a). It was found that arrivals from the basement suffer negligible variations in travel time, but undergo focusing effects which cause amplitude variations. Focusing in the final stages of a ray path introduces another amplitude modulation on the already complicated superposition of amplitude effects, a phenomenon noted in the oceanic setting by Purdy (1982). Defocused regions may reduce the amplitude of an arrival below detection threshold.

2.1.2 Salt domes

It was found that rays which had been 'chimneyed' up through the dome arrived at the surface about 0.7 s faster than their adjacent counterparts (Fig. 6b). Calculations indicate that the effect could be as much as 1 s. It is not clear from this simple model what other effects a mushroom-shaped salt dome with high impedance contrast might have.

2.2 SEISMOGRAM MODELLING

The crustal model for the North Sea presented here is unorthodox and requires explanation. The observed data indicated that there are no refractors between the base Zechstein and the Moho, and that there are large variations in crustal structure along the experimental line. These two features were incorporated into the model by representing the basement from pre-Permian level to Moho by a velocity gradient zone which varied continuously both horizontally and vertically.

2.2.1 Seismic velocity gradients

Refraction seismic interpretation was originally based on the premise that the Earth could be represented as a series of flat layers, each with constant seismic velocity, with general increase in velocities with depth (Ewing 1963). Two types of seismic phase, reflections and head waves, are associated with each interface, head waves forming the first arrivals at a seismometer. However, the amplitude of the head wave phase falls away rapidly after the

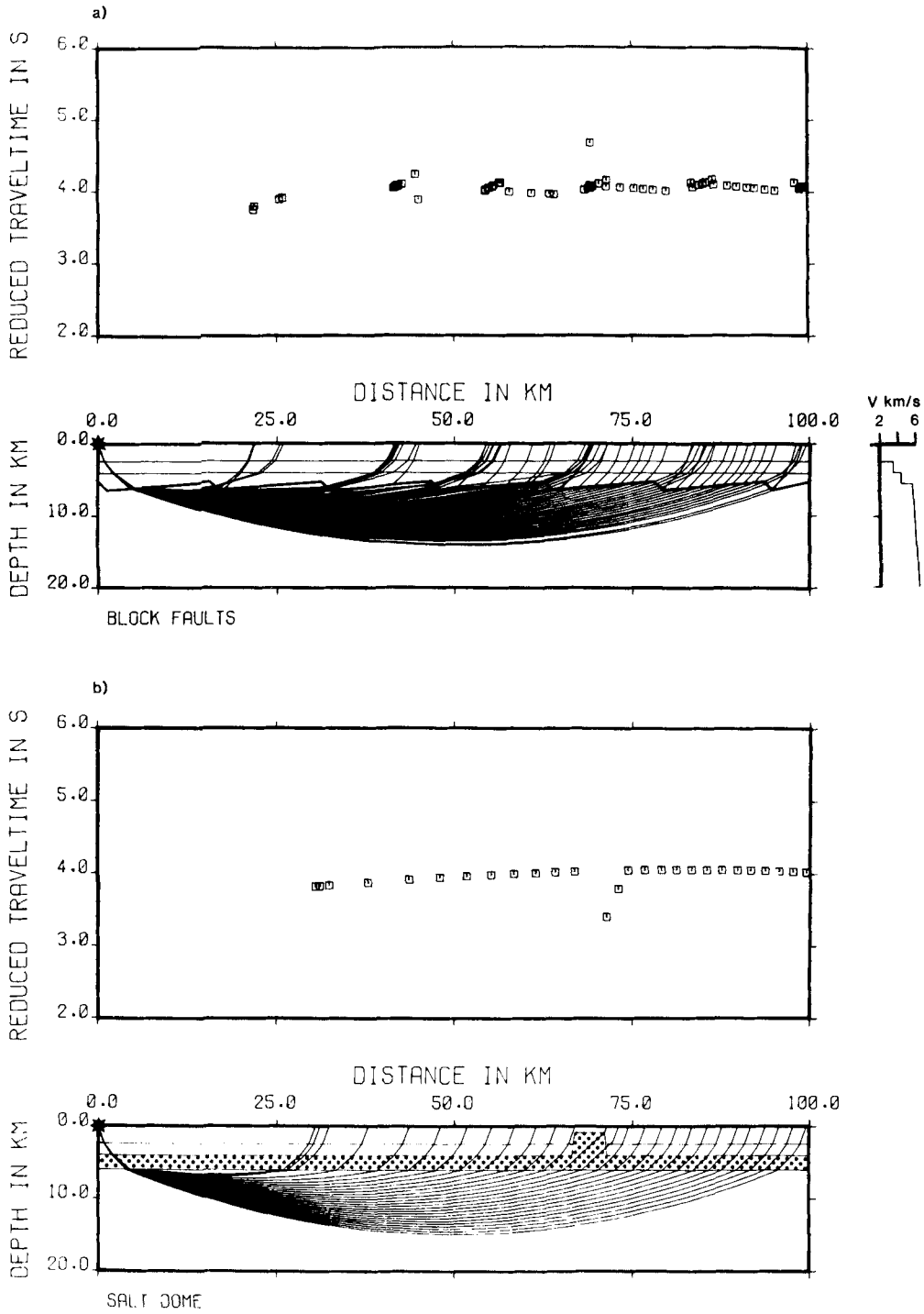

Figure 6. (a) idealized model of fault blocks in the North Sea basement. Beneath the faulted horizon velocity isolines are perturbed to simulate offset across faults at depth. The blocks cause small variation in travel times but focus the energy at particular ranges. (b) Idealized model of salt dome (salt layer stippled). The ray which has travelled up through the dome emerges at the surface 0.7 s earlier than the rays around it. Velocity structure similar to (a).

critical point (Heelan 1953) and it cannot actually be the type of ray recorded in long-range seismic refraction experiments.

Retaining the interface, but substituting a vertical velocity gradient for the homogeneous velocity field, energy is returned to the surface without undergoing reflection or critical refraction, producing a new class of arrivals called diving rays. A ray entering a gradient zone follows a curved path which may be viewed as continuous refraction across a stack of infinitesimally small layers (which is its representation in RAYSYN) or as a wide-angle reflection from a second order boundary, a fuzzy interface. The diving ray is not necessarily associated with interfaces, and produces strong arrivals which persist for a finite distance (Červený & Ravindra 1971), along curved branches on the travel-time plot. Unlike head waves, the branch terminates at a point related to the depth of the base of the layer.

Representing a seismic model purely as non-linear vertical velocity gradients, it will divide itself into sections which mimic a plane layered structure on the travel-time curve. These sections are delineated by changes in velocity gradient, and have associated pairs of prograde and retrograde branches analogous to the critical refractions and reflections respectively of a plane-layered model. The effect on the record section of changes to the velocity function with distance are similar to those with depth and when superimposed the two effects are difficult to distinguish.

The North Sea model started with few preconceived ideas of basement terrain, and so it was intuitively realistic, and conveniently flexible, to use continuous variation of both vertical and horizontal velocity gradients in the pre-Permian crust. The presence of sub-critical reflections is the only positive indication of a first-order interface (i.e. a rapid change in acoustic impedance in comparison with the signal wavelength). Only two first-order seismic interfaces were used in the model: the base Zechstein, represented as such for convenience, and the Moho.

2.2.2 *Amplitude modelling*

In addition to geometrical spreading, the observed amplitude of a seismic signal depends on a number of factors:

(1) velocity gradients, lateral and vertical,
(2) phase, and proximity to critical point,
(3) focusing effects of buried and surface topography,
(4) interference,
(5) attenuation.

The effects of gradients, phase, proximity to critical point and attenuation may be included in a RAYSYN model, but the resolution is not good enough to model fully either topography or interference. 1 km-square boxes cannot represent the small changes in surfaces which can cause amplitude fluctuations (e.g. the buried fault blocks discussed above; and Purdy 1982) but fortunately in the North Sea the greatest impedance difference, the sea bed, is virtually flat. The basin sediments have a significant absorption effect on seismic waves. Q has been measured in North Sea sediments (O'Brien & Lucas 1971; Stainsby & Worthington 1982); an average Q of 100 was used for all the sediments in the modelling. Q was set to 900 for the modelled pre-Permian crust and mantle (B. Kennett private communication).

The combination of (1) the complexity of the North Sea basin, (2) the complicated interaction of factors controlling amplitude, not all of which may be modelled, and (3) the quality of observations, meant that it was not feasible to model the details of amplitude

variations. In practice the match is usually quite successful, but it is optimistic to expect to reproduce variations in amplitude of a few per cent.

2.2.3 Assignation of phases

The first step in forward modelling of seismic data is the subjective identification of seismic phases (diving wave, head wave or reflection from a particular horizon) in the observed seismograms. By necessity the identification takes place early in the modelling, and then the model is changed until, if possible, it is made to generate the same phases synthetically, matching travel times and amplitudes, without generating other, spurious, arrivals. A bad choice of phase is quickly revealed by the modelling as impossible to achieve, but it is possible to be misled, perhaps permanently, by an inopportune interpretation. Criteria used in the choice include amplitude, waveform character, position of arrival on the travel-time branch, and the situation of the branch in the record section. In exceptionally quiet data, waveform polarity could also be utilized.

Preliminary raytracing through the depth-converted time-term solution revealed that Moho refractions generated by the model from shots east of the array did not emerge at the expected position on the travel-time branch, either in time or space. Evidently the Moho time-term solution had stabilized using arrivals from shots east of the Graben which should not have been interpreted as Moho refractions.

Most of the arrivals previously assigned as Moho refractions were re-interpreted as the crustal diving phase. This laterally persistent phase moves energetically across the array, often with an apparent velocity greater than $8.0\,km\,s^{-1}$, but frequently disappears before it reaches the other side. In some instances its initiation point may also be observed. The detailed modelling of this phase depends on small fluctuations in the velocity gradient in the crust, but its maximum persistence in distance marks the point where the crustal diving phase impinges on the Moho and becomes the retrograde Moho reflection. First arrivals at ranges greater than this cusp point are of small amplitude and have sub-Moho velocities. The position in time and space of the prograde crustal diving phase becoming the retrograde Moho reflection was found to be sensitive to both Moho depths and crustal velocities.

Thirty-two different models were raytraced before a good fit with the North Sea data was attained; only twice did the new model not show improvement over the old one.

2.2.4 Synthetic seismograms

Arrivals included on each seismogram were selected by hand; a procedure both quicker and more effective than using the program's automatic search routines. Tiny cusps within a larger phase, caused by lateral and vertical variations in velocity gradient, create amplitude instabilities in ray method calculations. These amplitude extremes were avoided by selecting an arrival which was representative of the bundle of rays emerging near the seismometer.

The waveforms in the observed data vary considerably from shot to shot, because they result from the interference effects of bubble pulse and water multiples from variable sized shots fired at less than optimum depth. This variation was simulated in the synthetics by convolving the calculated spike seismograms with a wavelet derived from the far-field records of each shot. Observed and synthetic seismograms have been scaled similarly to display 'true' amplitudes (see Table 1).

Synthetic seismograms were obtained for the 12 shots fired outside the receiver array. In each case the objective was to reproduce the main features of the observed record section. Three examples of these synthetic record sections are discussed below, with illustrations of the final model. Shot positions are indicated on Fig. 3. Small errors in modelled travel times

Table 1. Summary of amplitude scaling of observed and synthetic seismograms.

Observed data:

Recorded on 12 PUSSes of same design and setup
Similar physical environment
Shot weight equalization factor $W^{0.64}$
Trace amplitude multiplied by range
All observed seismograms low-pass filtered at 8 Hz

Synthetic seismograms:

Spike seismograms calculated by RAYSYN, convolved with:
Wavelets from observed data, each scaled between 0 and 1
Trace amplitude multiplied by range
No filter applied
Attenuation used in modelling:

North Sea sediments $Q = 100$
crystalline crust and mantle $Q = 900$

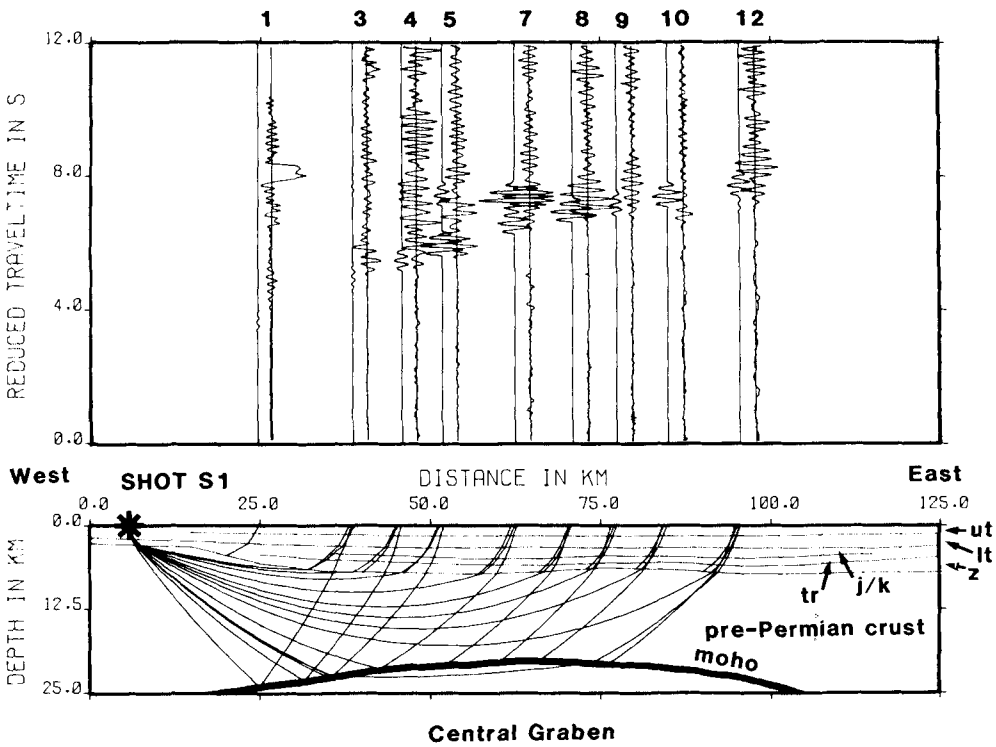

Figure 7. Ray diagram, observed and synthetic seismograms for shot S1. Each synthetic seismogram has the observed data reproduced alongside for comparison. The small-scale model of the Central Graben region (250 m-square boxes) allows detailed representation of the sediment horizons: ut, upper Tertiary; lt, lower Tertiary; j/k, Jurassic/Cretaceous; tr, Triassic; Z, Zechstein.

are probably due to the simplification of the sediment section. Observed and synthetic sections are reduced at 8.0 km s^{-1}.

Shot S1. Synthetic seismograms were obtained for shot S1 on both large and small model scales for comparison. The close range seismograms are at the limit of modelling using 1-km-square boxes and are better represented in the more detailed model (Fig. 7). The observed

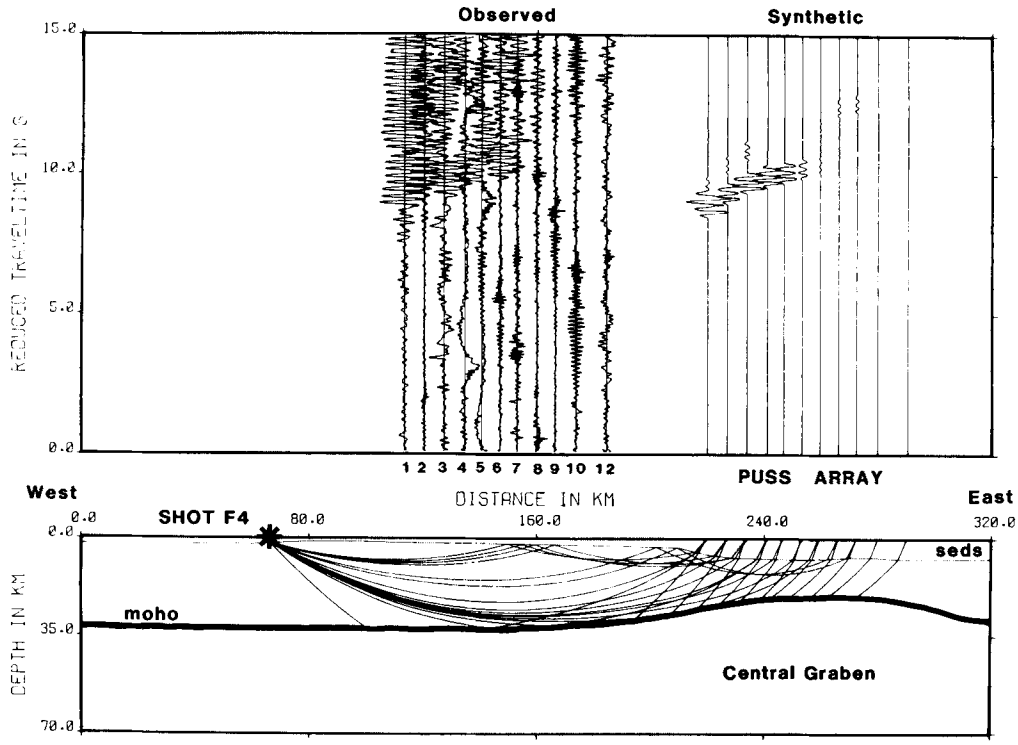

Figure 8. Ray diagram, observed and synthetic seismograms for shot F4.

arrival at PUSS 10 arrives relatively early due to a preferential raypath in the underlying salt dome. Otherwise, the travel time and amplitude pattern of the observations has been simulated satisfactorily. The agreement between the sets of synthetics from the two models was good enough to warrant the use of the large-scale, less detailed model for the rest of the shots, which all lie at greater ranges.

Shot F4. The main feature of the observed data is the high energy branch of arrivals with crustal velocities, which persists strongly until about half-way across the array and then disappears (Fig. 8). Sub-Moho arrivals were not identified. The strong arrival branch was interpreted as a combination of arrivals from rays turning in the lower crust, and from rays reflecting from the Moho. These two phases were of about the same amplitude after passing through the crustal gradients of the model, the reflections arriving slightly later. The position in time and space of this branch defines the velocity gradients in the crust; the distance at which the energy dies away fixes the position of the Moho. Observed and synthetic seismograms and a ray diagram are shown in Fig. 8. Fitting these modelled phases to the observed records constrained crustal structure in the region between about 120 and 260 km from the west end of the model (see Fig. 11). The model is designed so that mantle diving rays cannot reach the receivers from this shot. Energy from true head waves, as well as diving rays, is included in the modelling, but, as expected, arrivals are invisibly small on the synthetic seismograms.

Shot N1. The records from shot N1 (Fig. 9) are typical of those from the four shots (S6, S7, N1, S8) east of the Graben. Arrivals at PUSSes 12 and 10 are interpreted as being of the same phase, the Moho reflection, offset by different paths in the sediment. Arrivals at PUSS 9 mark the initiation of the crustal diving branch. The onset in space of this branch may be controlled by adjustment of the vertical velocity gradients in the upper crust. Using

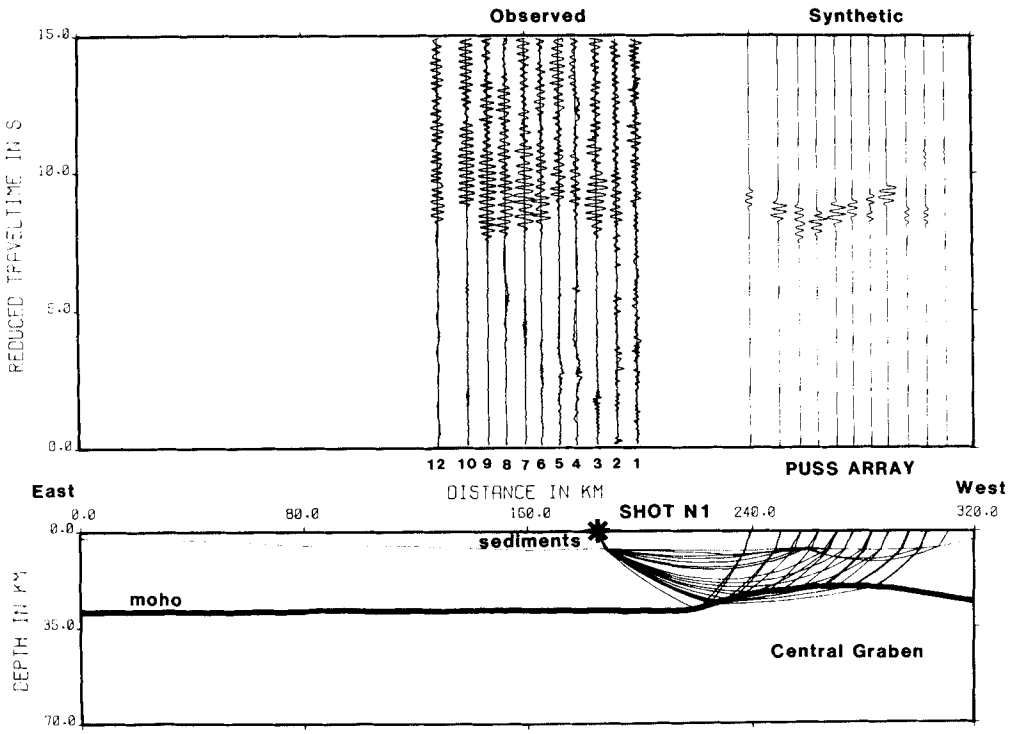

Figure 9. Ray diagram, observed and synthetic seismograms for shot N1.

this scheme, it was possible to obtain a good match between synthetic and observed data (Fig. 9). Although this complicated allocation of phases to observed arrivals is unsatisfactorily subjective, it was not possible to devise an alternative interpretation which better simulated the observations.

2.3 DESCRIPTION OF SEISMIC MODEL

2.3.1 Resolution of crustal structure

Finding one model which fits the data raises two questions:

(1) How well constrained is the model?

(2) Are there different models which would explain the data equally well? If so, how many?

Since the North Sea seismic model is not linearly related to the data it is impossible to answer the above questions quantitively. Perhaps a different interpretation of the seismic phases might allow a radically different model to be developed. No claim of uniqueness is made for this model of the North Sea; it is merely a possible model to explain data collected so far.

However, a useful qualitative feel for the resolution of each part of the model was obtained during modelling. Fig. 10 shows the model with all the raypaths used in the generation of the synthetic seismograms. At the edges there is no upper crustal information from the data and resolution is poor. However, in the region of the receiver array, and about 70 km either side, there is high information density and the structure is closely constrained

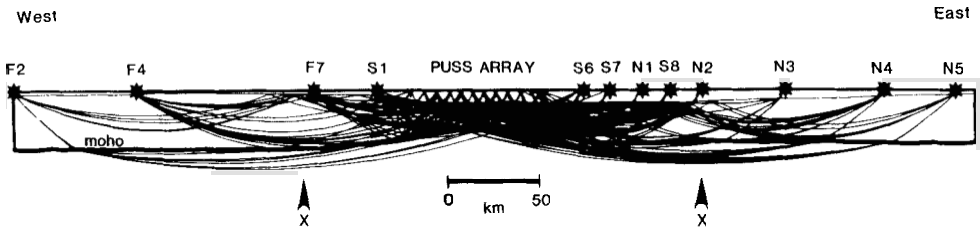

Figure 10. Final model with all raypaths used in the generation of synthetic seismograms. The sampling density is greatest in the central region XX where the Moho is constrained to within 1 km and the velocity structure to within about 0.1 km s^{-1}.

by the criss-crossing raypaths interpreted from the observations. In this central part, any change in Moho depth or shape by as little as 1 km significantly degrades the fit between synthetics and observations. A change in crustal velocities by as little as 0.1 km s^{-1} also causes a less good match.

2.3.2 Features of final model

The Moho is at about 32 km for the first 160 km distance along the model, and then shallows gently eastward to a depth of 20 km beneath the middle of the Central Graben (Fig. 11). The sediments make up about 7 km of the crustal thickness in this area, so that the pre-Permian basement is only 13 km thick. The Moho east of the Graben lies at about 29 km, about 3 km shallower than the west. Moho depths beneath the Central Graben line agree well with nearby crustal seismic models. The 32 km deep Moho beneath the west end of the model is 3 km shallower than the depth found on the LISPB profile in the Midland Valley of Scotland (Bamford *et al.* 1978). Beneath shot F7, the modelled Moho is deeper by 3 km than at the southern end of Christie's (1982) Main Line, situated 35 km north towards the Witchground Graben. East of the Central Graben the modelled Moho is compatible with analyses of CANOBE data (Cassell *et al.* 1983; S. Mykkeltveit private communication).

Fig. 11(a) shows velocity–depth curves projected at intervals across the model profile and Fig. 11(b) shows the velocity model contoured at intervals of 0.2 km s^{-1}. A general increase in crustal velocities by about 0.3 km s^{-1} occurs between shots F2 and F7. In the Central Graben area there is a high vertical velocity gradient (about 0.1 s^{-1}) in the thin pre-Permian basement. The crustal region beneath shots S6, S7, N1 and S8 consists of a low upper crustal gradient rapidly increasing to embrace a wide spectrum of velocities. A significant change in upper crustal velocity structure occurs near shot N2, constrained by the radical change in seismic character between records from adjacent shots (Barton & Matthews 1984). From shot N2 eastward the upper crust has high velocity and small gradient, but the gradient increases in the lower crust and velocities of more than 7.0 km s^{-1} occur above the Moho.

Sub-Moho velocity structures were not well resolved by the experiment. The general sub-Moho velocity of 8.1 km s^{-1} increases to 8.3 km s^{-1} in the upper 10 km of mantle. However, the raypath coverage in the mantle of the Central Graben area is sufficiently dense (Fig. 10) that the presence of a 'rift-pillow' with velocities of 7.5–7.8 km s^{-1} would certainly have been detected by this experiment.

3 Gravity interpretation

Gravity anomalies in the North Sea are small; Collette (1960) used this information to suggest isostatic compensation of the sediments. Donato & Tully (1981) calculated the

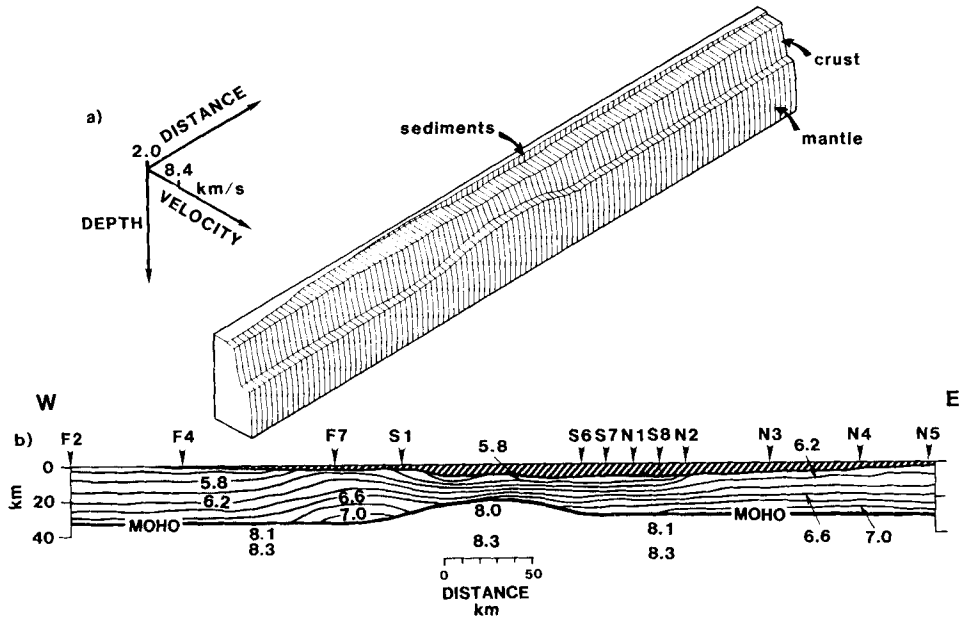

Figure 11. The final model. (a) Velocity–depth curves projected at intervals of 5 km along the model. (b) Model contoured to show velocity variation within the crust. Velocity contour interval 0.2 km s^{-1}. Sediments slashed. No vertical exaggeration.

gravitational effect of the density distribution in the sediments, and postulated compensation of the anomaly by thinning of the crust beneath the basin. Their analysis predicted a Moho depth decreasing to a minimum of about 20 km beneath the Viking and Central Grabens.

Gravity data are used here for two purposes:

(1) to show that the observed compensation of the sediments must occur locally, i.e. the sediments are supported isostatically rather than by the strength of the plate;

(2) to show that the seismic model, when converted to appropriate densities, is compatible with the observed gravity field.

Data were obtained from two sources:

(1) the published BGS Bouguer anomaly map (Donato & Tully 1981) of the British sector (Fig. 12a), supplemented by a single track along the seismic profile in Norwegian waters (G. Day private communication);

(2) satellite altimetry measurements of the geoid (SEASAT) were used to obtained a long-wavelength free-air gravity field (Fig. 12b) (Brennecke *et al.* 1982; D. McKenzie private communication).

Since variations in bathymetry are small, the difference between free-air and Bouguer anomalies is small. The two maps have a similar pattern but the anomaly map from altimetry contains only long wavelengths (> 30 km) and shows damping of anomaly amplitudes. Both anomaly maps show a smooth low-amplitude gravity field, with a small positive (about 20 mgal) following the graben system, flanked by shallow lows.

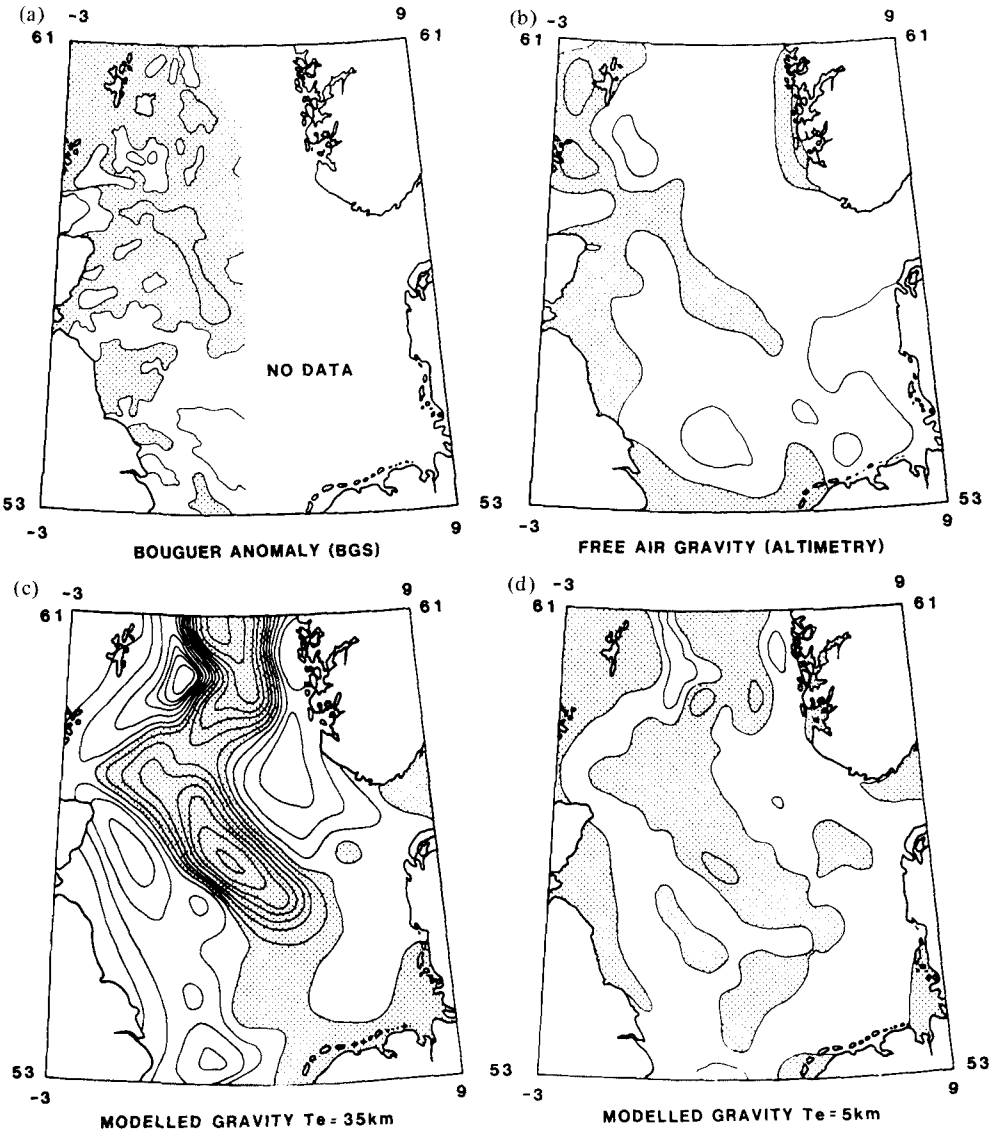

Figure 12. Gravity maps for the North Sea. Each map is contoured at 20 mgal intervals, and positive anomalies are shaded. (a) Bouguer anomaly map for the British sector (after Donato & Tully 1981). (b) Long wavelength free-air anomaly map from altimetry data. (c) Anomaly field generated by placing loads described in the text on a plate with elastic thickness 35 km. Note maximum positive of 150 mgal over Central Graben. (d) Anomaly field generated by placing same loads on plate with 5 km elastic thickness. The Central Graben positive is now reduced to a realistic 15–20 mgal.

3.1 SEDIMENT COMPENSATION

Studies of the geometry of deformation of the lithosphere in response to loading indicate that the plate will respond with a combination of flexural and isostatic compensation. If the lithosphere has lateral strength, governed by the elastic thickness of the plate, it responds not only to the load directly above, but also to the surrounding load. Conversely if the lithosphere has no lateral strength and zero elastic thickness it responds only to the load

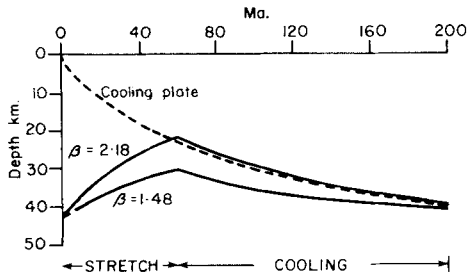

Figure 13. Depth of 450°C isotherm during and after an extensional event, after Jarvis & McKenzie (1980).

immediately above it, achieving equilibrium isostatically by the displacement of the weak fluid asthenosphere.

The amplitude and wavelength of observed anomalies generated in response to a known load on the lithosphere may be used to estimate the thickness of the part of the plate which has elastic strength (McKenzie & Bowin 1976; Watts, Karner & Steckler 1982). The net increase in load in the North Sea from end Cretaceous to the present day comprises three components:

(1) the sedimentary load of post Cretaceous infill (given by the maps of Day *et al.* 1981);

(2) the mantle load, due to thermal contraction of the lithosphere, obtained from the thermal subsidence of the basin since the Cretaceous;

(3) the load due to pre-sedimentation topography, given by the palaeobathymetric map for the late Cretaceous (see Fig. 18c).

The anomaly field generated by placing this composite load on plates of different elastic thickness was calculated and compared with the observed field. Initially the gravity field was modelled using an elastic thickness of 35 km. This estimate of the elastic thickness is defined by the position of the 450°C isotherm 40 Myr after the end of extension (Fig. 13). However, the magnitudes of the synthetic anomalies (Fig. 12c) were far greater than those observed, with the positive over the Central Graben reaching 150 mgal. The best fit to the observed gravity field was obtained using an elastic thickness of only 5 km, which reduced the anomaly over the Central Graben to 15–20 mgal (Fig. 2d). It proved difficult to model the steep gravity gradients observed around the western flank of the Viking Graben, due to the complicated pattern of sedimentation associated with the western boundary fault.

A plate with negligible elastic thickness cannot support large loads by flexure, thus the observed compensation of the sediments must occur locally.

3.2 VELOCITY–DENSITY MODEL

Laboratory measurements (Ludwig, Nafe & Drake 1970) show that rocks of each seismic velocity have a characteristic range of densities. A model defined in seismic velocities may be converted to typical densities by means of this relationship, and the gravity field of the model calculated. The North Sea seismic model must be consistent with the observed gravity field.

A 2-D density structure was used in the gravity modelling. The North Sea seismic model is composed of a matrix of over 37 000 boxes, each with a separate seismic velocity. Division of this model into a few simple prisms with uniform densities would destroy the essential variability of the structure. Instead, the *P*-wave velocity in each box was converted independently into an appropriate density, and the gravitational effect of the density matrix calcu-

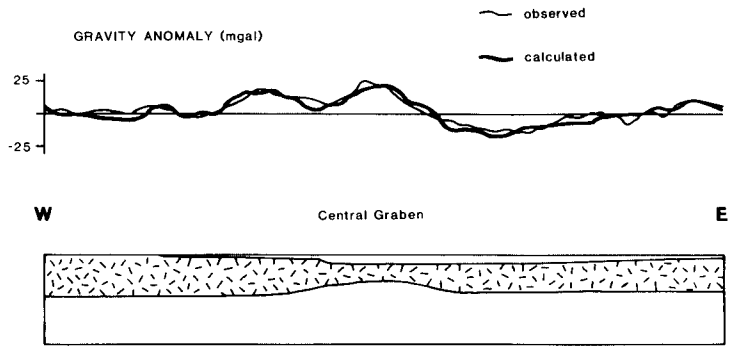

Figure 14. Calculated gravity anomalies (heavy line) for the 2-D North Sea model with the pre-Permian crust converted from velocities to densities as described in the text. The observed Bouguer profile (Donato & Tully 1981; G. Day private communication) is shown by a fine line.

lated. Sediment and mantle densities are comparatively well-known and were fixed in the calculations. Sediment densities were obtained for each stratigraphic unit in the North Sea from Donato & Tully (1981). A nominal density of 3.33 g cm^{-3} was used for all mantle with velocities greater than 8.05 km s^{-1}.

The velocity–density conversion in the pre-Zechstein crust was allowed to vary within the bounds of scatter on the Nafe–Drake curve (Ludwig *et al.* 1970). Using this approach, it was possible to model the calculated gravity profile to within about 5 mgal of the observed (Fig. 14). It was not possible to obtain a good fit using the mean of the Nafe–Drake relationship: crustal densities proved to be less varied than the velocity distribution would suggest. Instead, the velocity–density conversion function varied along the line. Since the complete line extends 530 km distance, crossing continental blocks with various histories (Smythe, Skuce & Donato 1980), it is not surprising that a single-valued velocity–density relationship cannot be applied along its whole length. The lateral stress variation at the base of the density model has a wavelength of about 160 km and amplitude about 300 bar; within the range of stresses expected in the crust (Garland 1979).

4 Subsidence study

The stretching model may be used to predict the subsidence path of the basement in a basin formed by a stretching event of given rate and duration (Jarvis & McKenzie 1980). These theoretical paths may be compared with data from exploration wells in order to estimate the implied extension.

The subsidence of the basement is recorded by the sediments which accumulate in the basin, but these sediments load the lithosphere and cause more subsidence than if the stretched basin had been filled with water alone, which is the assumption of the model. Therefore the tectonic part of the subsidence is isolated by correcting the basement subsidence path for sediment and water loading at different times.

Subsidence paths have been calculated using data from 19 wells (Fig. 15) and maps of sediment thickness (Day *et al.* 1981). Since all wells are drilled on structures suitable for the discovery of oil or gas, generally over structural highs, the succession is often incomplete or condensed, and hence atypical. Where possible wells with the most complete geological section have been studied (Figs 15, 16). The wells have been backstripped and unloaded following the method of Steckler & Watts (1978). This technique requires detailed information on stratigraphy, palaeobathymetry, changes in sea-level, sediment compaction and the basement response to loading at different times during the history of the well.

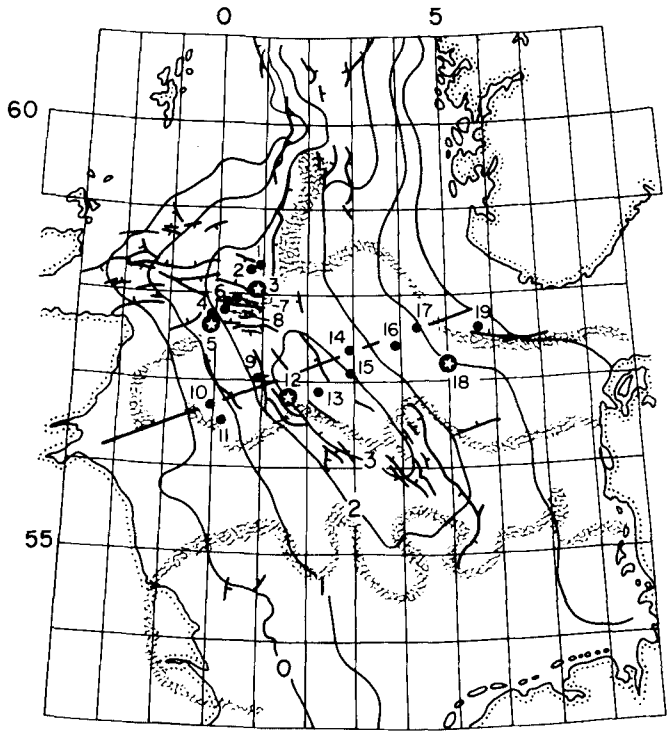

Figure 15. Map showing positions of exploration wells used in subsidence study. Numbered dots, well sites; heavy line, refraction profile and sediment cross section; fine lines, Tertiary isopachs in kilometres; ticked lines, major faults; hatched border, limit Zechstein salt. The positions of the four wells to be discussed in detail are highlighted with star symbols.

Key to wells

1 – BP 15/20-1. 2 – BP 15/24-1. 3 – Conoco 15/30-1. 4 – BP 20/10-1. 5 – BP 20/10-2. 6 – BP 21/2-1. 7 – BP 21/2-4. 8 – BP 21/6-1. 9 – Shell 21/30-1. 10 – Amoco 27/10-1. 11 – BP 28/12-1. 12 – Shell 29/3-1. 13 – BNOC 30/2-1. 14 – Conoco 7/9-1. 15 – BP 7/12-3a. 16 – Conoco 8/12-1. 17 – Conoco 9/4-3. 18 – Shell 9/12-1. 19 – Conoco 10/5-1.

4.1 STRATIGRAPHY

An accurate stratigraphy is necessary to reconstruct the sedimentary section as it developed during the evolution of the basin. The wells were subdivided using biostratigraphy based on the occurrence of foraminifera separated from drill cuttings (Jenkins & Murray 1981), and lithostratigraphy based on geophysical log characteristics (Deegan & Scull 1977). Because of uncertainty due to the sampling interval in the wells (often greater than 100 ft) and problems associated with caving, lithostratigraphic picks were used in preference to biostratigraphy.

The stratigraphic subdivision of the wells is summarized in Fig. 16. In the majority of the wells middle Jurassic or younger deposits lie unconformably on Triassic or older units (i.e. lower Jurassic is absent), except well 15 where Lias is present. The Callovian and Oxfordian appears to be absent in all wells, although it has been reported present elsewhere in the North Sea (Deegan & Brown 1981). During the middle Jurassic and Early Cretaceous faulting strongly influenced sedimentation and erosion patterns, resulting in incomplete sections in all the wells. Continuous sedimentation from the Jurassic to the Cretaceous only

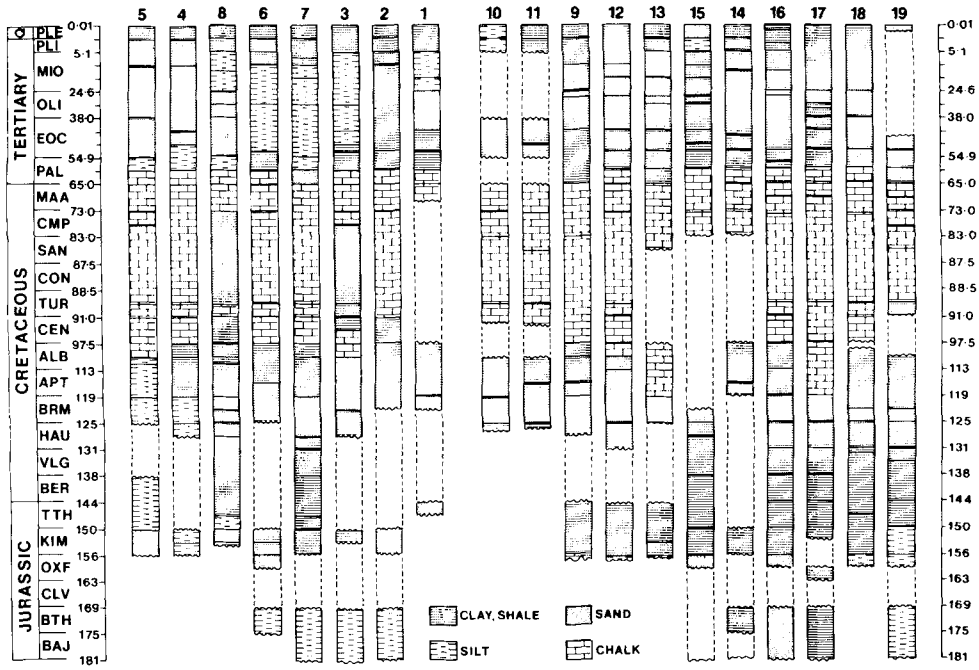

Figure 16. Summary of stratigraphy and lithology for the wells studied.

occurs in a few wells, elsewhere the Base Cretaceous unconformity separates the two periods. The subdivision of the early Cretaceous and Jurassic is based mainly on palynology since the formation boundaries are diachronous and there are few foraminifera.

Sedimentation was generally continuous from the middle Cretaceous, although some wells in the Central Graben (13, 14, 15) have been affected by salt movement. Hancock (1981) suggests that the Fladen Ground Spur did not become submerged by the Chalk Sea until Campanian times, which would account for the reduced Late Cretaceous section in well 1. The missing sections in the more marginal wells (19, 10, 11) are probably due to erosion during times of low sea-level or glaciation.

Stratigraphic information was converted to time using the new time-scale of Harland *et al.* (1982).

4.2 PALAEOBATHYMETRY

The depth of water at the time of deposition of the sediments, the palaeobathymetry, has been estimated by comparing fossil foraminiferal assemblages from drill cuttings with assemblages found in known environments in present-day oceans. These comparisons may only be made on a generic level since few of the fossil species found in the North Sea extend into the Holocene. Studies of the distribution of present-day foraminifera in the Gulf of Mexico (Phleger 1951, 1960; Parker 1954; Pflum & Frerichs 1976; Walton 1964; Bandy 1954, 1956) have shown that assemblages may be used as water depth indicators. These distribution patterns were used as a guideline to supplement the benthonic foraminiferal distribution patterns observed on the European seaboard (Table 2). Where foraminiferal evidence is sparse palaeogeographical and ecological evidence have been used to help determine the palaeowater depths.

Table 2. Depth distribution of foraminifera on the European seaboard and other temperate shelf seas.

INNER NERITIC 0-30m		
Elphidium 6,7	Protoelphidium 7	Bolivina 7
Cibicides 7	Haplophragmoides 7	Quinqueloculina 7
Ammonia 7	Fursenkoina 7	Textularia 7
MIDDLE NERITIC 30-100m		
Bulimina 1,3,7,9	Trochammina 2,7, 9	Quinqueloculina 7,9
Fursenkoina 1,3,9	Cibicides 1,2,7,9	Nonion 3,7
Eggerella 1,3,5,7,8,9	Textularia 1,2,5,7,9	Elphidium 6,7,9
Cribrostomoides 2,7,9	Ammonia 3,6,7,9	Reophax 3,6,7,9
Protoelphidium 5,7	Bucella 5,7,9	Guadryina 2
Pyrgo 7,9	Dentalina 7, 9	Spiroplectammina 5,6,9
Bolivina 7,9	Rosalina 7	Asterigerina 7
Eponides 7	Haplophragmoides 7	Cassidulina 9
Ammodiscus 9	Angulogerina 9	Lenticulina 9
Polymorphinids		
OUTER NERITIC 100-200m		
Bulimina 6,7	Textularia 4,5,7	Melonis 5,7
Cassidulina 4,5,7,8	Bucella 5	Haplophragmoides 7
Martinottiella 4,7	Spiroplectammina 5	Marginulina 8
Fursenkoina 4	Recurvoides 5	Uvigerina 8
Cibicides 7	Globocassidulina 7	Trochammina 7
Cribrostomoides 7		
UPPER BATHYAL 200-600m		
Cassidulina 5,7,8	Bulimina 3	Trochammina 7
Recurvoides 5	Cyclammina 7	Cribrostomoides 7
Melonis 5,7	Uvigerina 7	
MIDDLE BATHYAL 600-1000m		
Cyclammina 7	Uvigerina 7	Cassidulina 7
Melonis 7		

1 = Bristol Channel, 2 = English Channel, 3 = Plymouth Sound, 4 = Celtic Sea, 5 = Hudson Bay, 6 = Baltic and North Seas, 1–6 all in Murray (1973), 7 = British Isles (Murray 1971), 8 = Eastern USA Maine to Maryland (Parker 1948), 9 = New Jersey continental shelf USA (Poag, Harley & Todd 1980).

There is little palaeontological evidence from the Jurassic. Assemblages typical of Haig's (1979) *Ammobaculites* association were found in the shales; the lack of calcareous fauna suggests a restricted environment. The Jurassic sands contained no foraminifera but yielded shell fragments and glauconite. A gradual deepening is inferred throughout the Jurassic, with shallow marine/deltaic sands deposited on the highs, passing laterally and vertically upwards into darker marine shales deposited on a broad undulating topography.

The majority of Cretaceous samples yield poor assemblages due to the common practice of turbo drilling these horizons. The dark shales and silts of the Lower Cretaceous contain assemblages of agglutinated foraminifera similar to those in the Jurassic. During the Barremian conditions became slightly more marine with deeper water indicated by a higher proportion of calcareous benthonic and planktonic foraminifera. Assemblages from the mid-Cretaceous contain a high proportion of either planktonics (90 per cent) or agglutinates (95 per cent). This bimodal distribution is thought to be related to the development of an oxygen minimum zone above the sediment–water interface (Schlanger & Jenkyns 1976). The agglutinated assemblage contains similar genera to Haig's (1979) *Marsonella* association, while the presence of planktonics suggests outer shelf conditions. The upper Cretaceous chalk facies contain faunas comparable with the upper slope faunas of the Cretaceous of California (Scliter & Baker 1972) with water depths in excess of 100 m. Evidence of slumping suggests deeper water conditions in the grabens.

During the Tertiary the North Sea basin gradually infilled with sediments, with the shallowing reflected in the foraminiferal assemblages. In the Palaeogene (Upper Palaeocene–

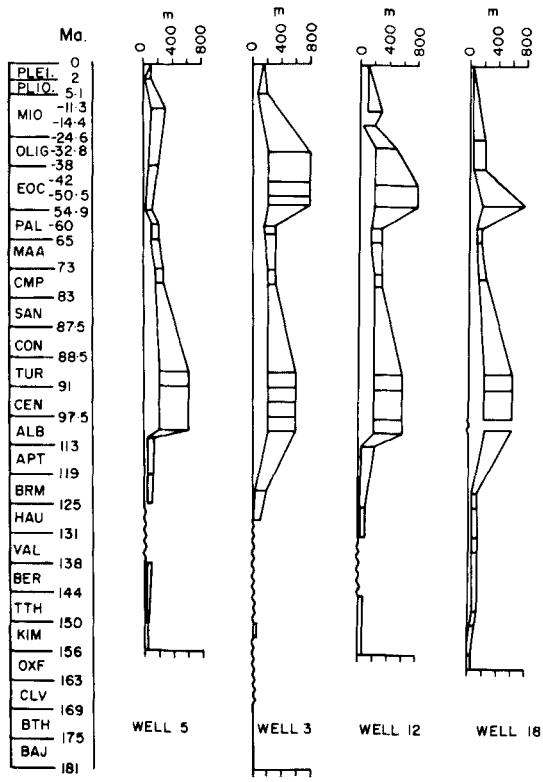

Figure 17. Estimates of changes in water depth through time for four of the wells studied. A range of depths is inferred for each sample, due to uncertainties in depth determination.

Oligocene) deeper water conditions existed within the grabens, with a delta fan complex prograding out from the East Shetland platform (see Fig. 18b). The well samples contain a typical flysch-type agglutinated fauna indicating a carbonate poor environment where calcareous forms were restricted. The minimum depth necessary to maintain such an environment is over 200 m, well below wave base. A maximum water depth of 1000 m is given by seismic stratigraphy and palaeoslope studies (Sutter 1980; Rochaw 1981). As the basin filled and shallowed the flysch-type assemblage was replaced by assemblages containing a diverse calcareous fauna. By Pliocene times the North Sea basin was almost completely infilled with very shallow conditions indicated by *Elphidium* rich assemblages (Murray 1973).

The changes in water depth for four of the wells are shown in Fig. 17. Because of the uncertainty in the water depth determinations a range of depth is inferred from each sample. Maps of palaeobathymetry (Fig. 18) were constructed for various time intervals, by combining information obtained from the well samples with the palaeogeographic maps of Ziegler (1981, 1982a). These maps show that during the Early Cretaceous an archipelago of islands developed on the foot wall blocks of the normal faults bordering the Central Graben (Fig. 18d). A similar topography is seen today in the Aegean Sea, where uplift on the foot wall blocks of large normal faults can account for Neogene palaeogeography and distribution of deposits in the Isthmus of Corinth (Jackson *et al.* 1982).

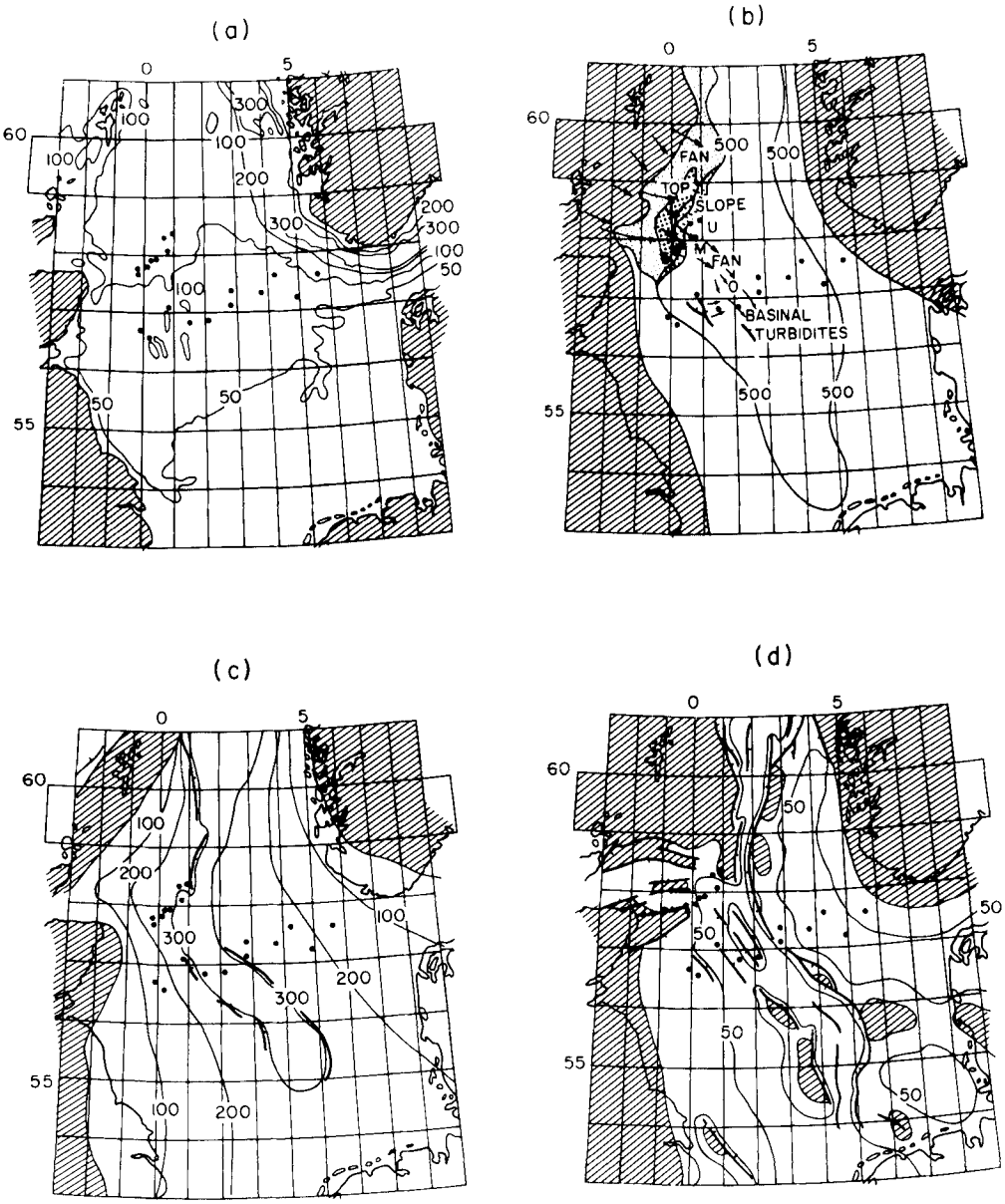

Figure 18. Palaeobathymetric maps of North Sea for various time intervals: (a) present day, (b) Palaeocene, (c) Late Cretaceous, (d) Early Cretaceous. Note the archipelago of islands bordering the Central Graben in the Early Cretaceous resulting from uplift of foot wall blocks of large normal faults.

4.3 SEA-LEVEL

Sea-level is the reference height for all subsidence calculations, and therefore changes in eustatic sea-level should be accounted for. However, although sea-level is believed to have varied during the geological interval under study, there is little consensus in the literature about the magnitude and frequency of these changes.

Pitman (1978) obtained a sea-level curve based on volume changes of the mid-ocean ridge system which shows a fall in sea-level since the mid-Cretaceous. The curves of relative

changes of sea-level produced by Vail, Mitchum & Thompson (1977) are based on inter-regional stratigraphic studies and exhibit a primary cycle, calibrated to Pitman's curve, with a rise in sea-level in the Cretaceous reaching 350 m during the Campanian, followed by a gradual fall to the present day. Superimposed on this sea-level curve are secondary and tertiary cycles of shorter duration.

Watts & Steckler (1979) analysed the subsidence history of five deep wells on the continental margin of eastern North America. They isolated the eustatic effect by removing the effects of depth of deposition and tectonic (thermal) subsidence. The resulting curve gives a maximum elevation of 150 m in the Late Cretaceous and is of similar magnitude to the range of sea-level elevations computed by Bond (1978).

Pitman's (1978) sea-level curves were calculated using an old time-scale (Anonymous 1964; Berggren 1969) now superseded by the time-scale of Harland *et al.* (1982) used here. Pitman's (1978) data, based on volumes of mid-ocean ridges, cannot simply be replotted to the new time-scale; the relationship is non-linear. Because of the lack of consensus over the magnitude and frequency of sea-level variations, and because of the problems of using different time-scales from those used here, sea-level variations were not included in this study; sea-level was assumed to have remained at its present level. Implications of ignoring this fluctuating sea-level are discussed later (Section 5, Fig. 22).

4.4 DECOMPACTION

To correct the sedimentary loading effects on the basement it is necessary to know the sediment thickness and the mean sediment density for the total sediment pile at any time. As the sediments are progressively buried the pore fluids are expelled and the sediment thickness decreases. The mean density of the sediment pile also changes as a consequence of this compaction, since as the fluid is expelled the mean density of the sediment approaches the sediment grain density. The effect of sediment compaction through time must be calculated and reversed.

The wells were subdivided by lithology into sand, shale, sandy shale (silt) and chalk units (see Fig. 16). Triassic and older units were assumed to have been completely compacted prior to the Middle Jurassic; all younger units were progressively decompacted using the method described by Sclater & Christie (1980). All except four wells intercepted Triassic or older units; in these wells the basement level was estimated from depth-converted seismic sections (P. Ziegler private communication) or from the isopach maps of Woodhall & Knox (1979).

The model of decompaction developed by Sclater & Christie (1980) is based on the simple porosity–depth relationship of Ruby & Hubbert (1960). As each layer is removed during backstripping the top of the next unit is brought to the surface and the remaining sedimentary column below is decompacted to its thickness in the absence of that overburden, allowing for differences in lithology in the section. Decompacted and undecompacted subsidence curves for four wells are shown in Fig. 19(a). The effect of decompaction is to increase the depth to basement at each time.

4.5 BASEMENT RESPONSE TO LOADING

Assuming local loading (see Section 3) the basement was unloaded using the general equation of Steckler & Watts (1978):

$$y = S^* \frac{(\rho_m - \rho_s)}{(\rho_m - \rho_w)} - SL \frac{(\rho_m)}{(\rho_m - \rho_w)} + WD$$

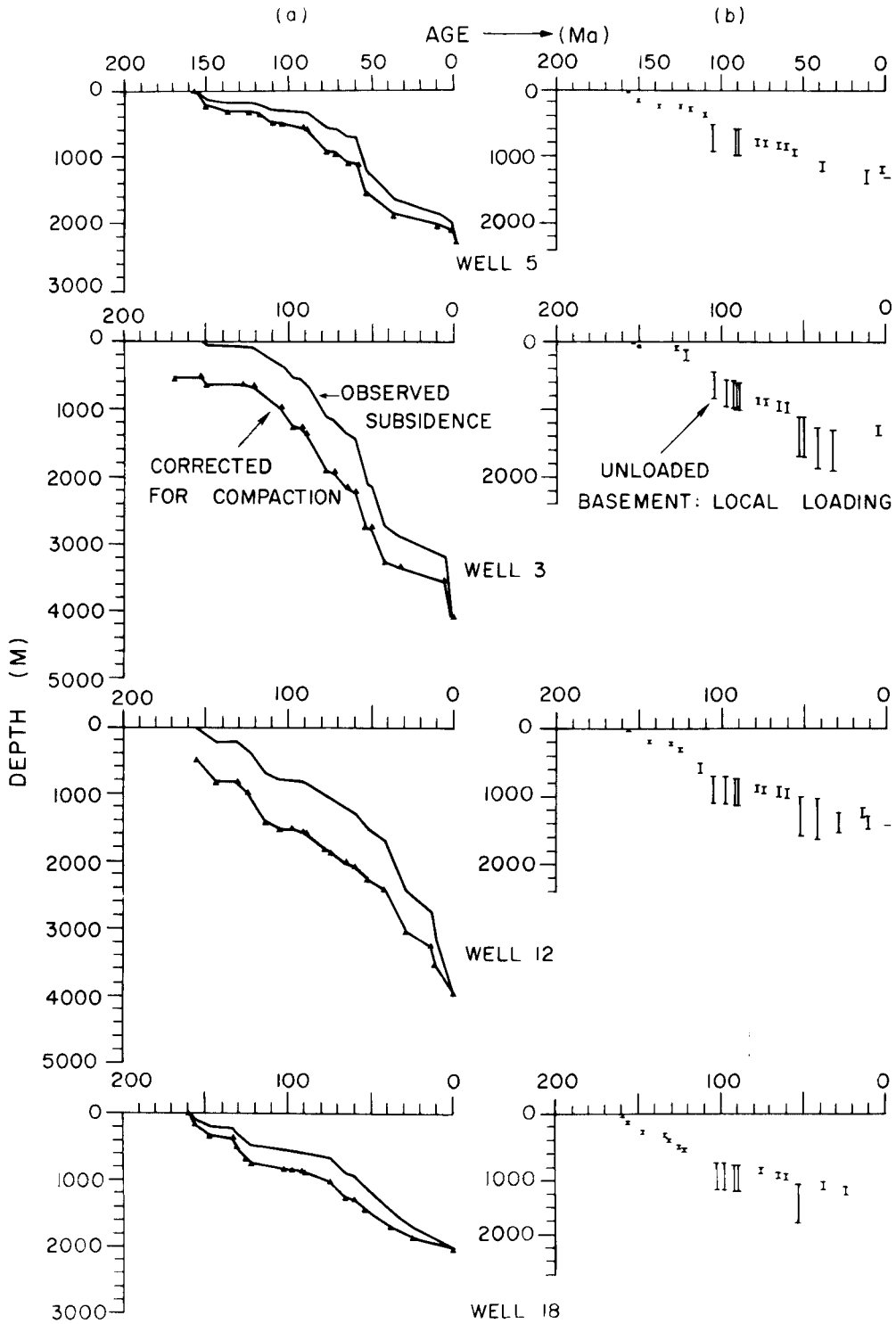

Figure 19. Decompaction and backstripping of four wells. (a) Observed basement subsidence paths (upper line) are corrected for compaction (lower line with triangles). The effect of this correction is to increase depth to basement at each time. (b) Subsidence paths (depth to basement) corrected for sediment and water loads. These values show basement subsidence for a basin filled only with water. The uncertainties in water depth for each sample mean that there is a range of possible depths to basement at each time.

where y is the depth to the basement in the absence of sediment and water loads, S^* is the sediment thickness corrected for compaction, ρ_s, ρ_m and ρ_w are the mean densities of the sediment, mantle and seawater respectively, SL is the sea-level relative to the present day (here assumed to be zero) and WD is the depth of deposition, i.e. the palaeobathymetry.

The position of y (depth to basement) back through time in four of the wells is shown in Fig. 19(b). It was assumed that deposition of the oldest post-Triassic deposits in each well occurred close to sea-level. The value of y for this oldest deposit was thus set to zero, and all other basement depth values plotted relative to this zero point. Because of the uncertainties in the palaeobathymetry there is a range of possible values for y at each time constrained by maximum and minimum possible water depths. Slower subsidence and less total subsidence is seen in the more marginal wells (e.g. 5 and 18) than those from the centre of the basin (e.g. 3 and 12).

4.6 RESULTS

Tectonic subsidence curves were obtained for each well using the methods discussed above. These observed curves are compared with theoretical curves generated using the method of Jarvis & McKenzie (1980) using a model modified to include the crust so as to give initial (isostatic) subsidence as well as the thermal component. Computations were made assuming a 60 Myr period of extension from the mid-Jurassic to early Cretaceous, followed by passive subsidence until the present day. It was assumed that the thermal effects of any earlier stretching events had decayed by mid-Jurassic times.

The theoretical curve was chosen to give the closest fit to the thermal part of the subsidence while not exceeding the amount of initial subsidence apparent in the well. Initially, all observed subsidence curves were compared with theoretical curves generated assuming a pre-stretching crustal thickness of 31 km and a crustal density of 2.8 g cm^{-3} (after Cochran 1982). Although a good fit was obtained for the marginal wells, it was not possible to fit these theoretical curves to the observed subsidence data from wells in and near to the

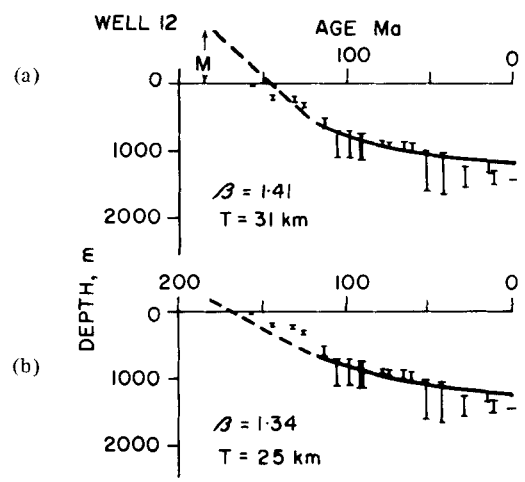

Figure 20. Subsidence data for well 12. (a) Theoretical curve generated assuming initial crustal thickness of 31 km fits the thermal subsidence well but makes an unacceptable mismatch (M) between the observed and predicted initial subsidence. (b) Theoretical curve recalculated using a smaller initial crustal thickness (25 km), fits the thermal subsidence equally well, but reduces the mismatch between observed and predicted initial subsidence to an acceptable level.

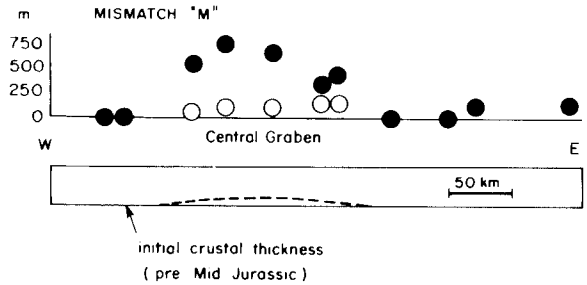

Figure 21. Values of M, the mismatch between observed and predicted initial subsidence, plotted for various assumed initial crustal thicknesses. Well positions are projected on to a crustal cross-section beneath the refraction line. Closed circles show mismatches for uniform 31 km thick pre-mid-Jurassic crust, open circles show reduced mismatches obtained using the modified crustal profile indicated by a broken line below. The data fit best a model in which the crust is already slightly thinned beneath the Central Graben at the time of the mid-Jurassic extension event.

Table 3. Best-fit parameters for subsidence curves for central North Sea wells. All calculations assume a 60 Myr period of extension from mid-Jurassic to early Cretaceous, followed by thermal subsidence to the present day. Assumed mean crustal density 2.80 g cm^{-3}.

Well number	Pre-stretching crustal thickness (km)	Estimated β
1	28	1.3
2	28	1.3
3	28	1.3
4	28	1.3
5	28	1.3
6	28	1.4
7	28	1.3
8	28	1.4
9	28	1.2
10	31	1.1
11	31	1.1
12	25	1.35
13	25	1.55
14	28	1.35
15	28	1.2
16	31	1.2
17	31	1.2
18	31	1.2
19	31	1.2

Central Graben; here the calculated amount of initial (faulted) subsidence for a given amount of thermal subsidence was much greater than that observed. An example of this problem is illustrated for well 12 in Fig. 20(a). The theoretical curves were recalculated for the central wells using smaller values for the initial crustal thickness, which reduces the predicted initial subsidence, and good agreement was obtained between observed and calculated subsidence paths (Fig. 20b). The mismatches (M) between the observed and calculated subsidence paths in all the wells are shown for both the uniform 31 km thick

crust and the modified mid-Jurassic crustal profile in Fig. 21. The modified mid-Jurassic crustal profile, with slight residual thinning beneath the Central Graben, reduces the mismatches between observed and predicted initial subsidence to a negligible amount. Stretching factors and model parameters are shown in Table 3.

5 Discussion

5.1 THE EFFECT OF SEA-LEVEL CHANGES ON THE SUBSIDENCE DATA

We assumed in the subsidence study that eustatic sea-level did not change during the period studied. We here discuss the effect that fluctuations of sea-level might have on the interpretation. Returning to the subsidence equation:

$$y = S^* \frac{(\rho_m - \rho_s)}{(\rho_m - \rho_w)} - SL \frac{(\rho_m)}{(\rho_m - \rho_w)} + WD$$

values of y, depth to basement, were replotted using values of SL for different times taken from Watts & Steckler (1979) (Fig. 22a). The rise in sea-level during mid-Cretaceous times causes pull-up of the basement depth values resulting in an apparent decrease in subsidence rate for this time. No significant difference is made to the value of β for the subsidence curve which best fits the data (Fig. 22), but the goodness of fit is reduced in the case where sea-level changes are included. The general effect of including variations in sea-level in the North Sea subsidence data is to introduce apparent fluctuations in the subsidence rate; the smoothest subsidence curves were obtained assuming constant sea-level. These observations suggests either that some additional, unconsidered factor has influenced subsidence patterns in the North Sea basin, or that the sea-level curves of Vail *et al.* (1977) and Watts & Steckler (1979) are not reflecting true global changes in sea-level.

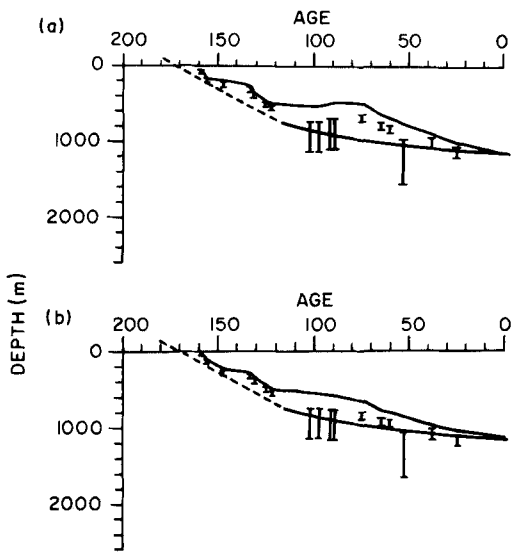

Figure 22. (a) Subsidence data for well 18 corrected for estimated changes in eustatic sea-level (Watts & Steckler 1979). (b) Same data with no eustatic sea-level correction. The general effect of including variations in sea-level is to introduce apparent fluctuations in the subsidence rate, but the implied stretching factor does not alter. On each figure; upper continuous line, basement subsidence corrected for sediment loading and sea-level: error bars, subsidence after adding water-depth correction: lower continuous/dashed line, best fit model subsidence curve.

5.2 ESTIMATES OF STRETCHING OF THE LITHOSPHERE

We have described seismic and subsidence studies designed to test the stretching model for the formation of the North Sea basin. Here we compare the results of those tests. The subsidence data were shown to fit best a model in which the crust beneath the Central Graben was already slightly thinned at the time of the mid-Jurassic extensional event. Estimation of stretching factors from the seismic model depends on assumptions about crustal history. Assuming that extension was in the plane of the crustal section, i.e. approximately perpendicular to the Central Graben, the simplest additional assumption is that the crust had a uniform thickness of say 31 km before any basin formation took place. However, in the North Sea area, basin formation was preceded by a major orogeny, and it is difficult to envisage a pre-stretching crust uniform across the width of the basin (Smythe *et al.* 1980). An alternative assumption, adopted here, is that isostatic equilibrium was maintained throughout the history of the basin as it is today (see Section 3).

Assuming that isostasy was maintained, with basement close to sea-level, it is possible to construct crustal profiles for successive steps backward in time and so to estimate stretching factors. The present-day crustal model was divided into narrow isostatic columns (Fig. 23). The top sedimentary time unit was removed, and the crust thickened in isostatic adjustment. This thickening was effected by horizontal shortening of the column in the plane of section, assuming that crust was conserved. Stretching factors were calculated by comparison of 'before' and 'after' crustal thicknesses.

The uncertainties in this type of reconstruction are formidable, arising partly from uncertainties in the model of the present-day crust, but to a much greater extent from assumed mean densities of the sediment (2.2 g cm^{-3} from Donato & Tully 1981), pre-Permian crust (2.8 g cm^{-3}), and mantle (3.3 g cm^{-3}). Table 4 shows the range of β-values and reconstructed crustal thicknesses calculated for the assumed mean densities above and for estimated uncertainties in mean densities (sediments ±0.20 g cm^{-3}, crust ± 0.05 g cm^{-3},

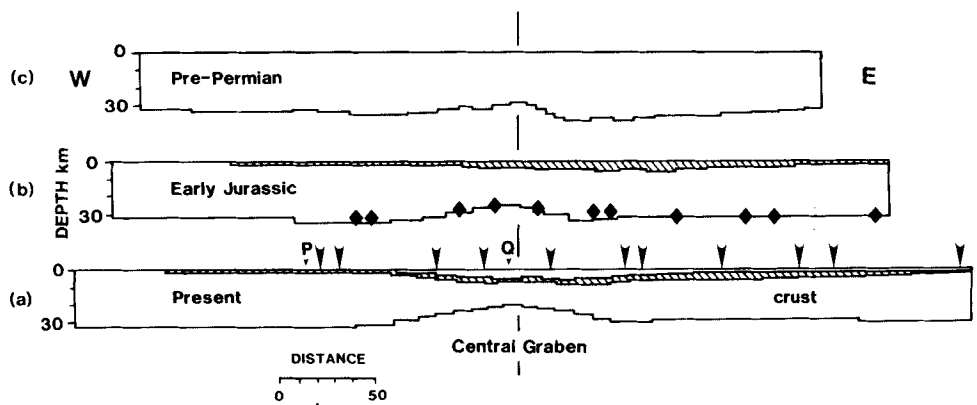

Figure 23. Isostatic crustal reconstruction for successive geological periods. The uncertainties in this reconstruction are formidable, and vary across the width of the basin. These uncertainties are tabulated for points P and Q, typical of the margins and centre of the basin respectively, in Table 4. (a) Present-day crustal structure, determined by seismic refraction, divided into narrow isostatic columns. Well positions shown by arrows. (b) Reconstruction of early Jurassic profile obtained by removing post-mid-Jurassic sediments and thickening and shortening each column in isostatic compensation. Diamonds show best fit pre-mid-Jurassic crustal thicknesses determined from well subsidence data (see Fig. 21). Size of diamonds indicates approximate uncertainties. (c) Reconstruction of pre-Permian crustal profile.

Table 4. Summary of uncertainties in isostatic crustal reconstruction and β-values at points P and Q on Figs 23 and 24 due to uncertainties in assumed densities of sediments, crust and mantle. Uncertainties due to resolution of seismic experiment are small by comparison.

Assumed densities: sediment $\rho_s = 2.20 \pm 0.20\,g\,cm^{-3}$
crystalline crust $\rho_c = 2.80 \pm 0.05\,g\,cm^{-3}$
mantle $\rho_m = 3.30 \pm 0.10 g\,cm^{-3}$

Position on Figs 23 and 24	Basin margin (P)		Basin centre (Q)	
Densities used in isostatic reconstruction	Mean ρ	Extreme ρ	Mean ρ	Extreme ρ
Mid-Jurassic Moho depth (km)	33.0	32.4–34.0	24.7	22.3–28.1
Pre-Permian Moho depth (km)	34.0	32.9–36.1	28.0	23.8–37.0
Post-mid-Jurassic β	1.06	1.04–1.09	1.64	1.49–1.88
Total β	1.12	1.09–1.19	2.18	1.83–2.85

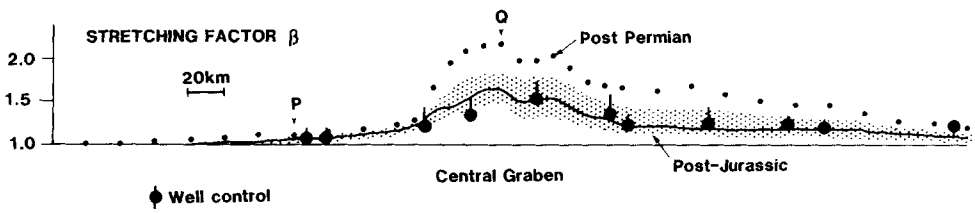

Figure 24. Plot of estimated β-factors for different positions along the present-day crustal profile. Post-mid-Jurassic stretching factors from well data are shown by large black dots: estimated uncertainties indicated by vertical bars. The thin line shows the variation in post-mid-Jurassic stretching factors estimated from the reconstructed crustal profile (Fig. 23), the stippled region around this line is a measure of uncertainties due to assumed densities of sediments, crust and mantle (see also Table 4). The net post-Permian stretching implied by the crustal reconstruction is shown by the dotted line. The uncertainties in the crustal reconstruction are considerable (Table 4), even if the Permo-Trias event is simply an extension in the plane of section.

mantle $\pm 0.10\,g\,cm^{-3}$) for two representative sites chosen in the centre and on the flank of the basin. These errors are largest where the crust is thin and the sediment thick, so that the less certain densities dominate.

Both the subsidence studies and the isostatic reconstruction described above give estimates of the pre-mid-Jurassic crustal thickness, and of the stretching which took place during the mid-Jurassic to early Cretaceous event. Both parameters vary across the width of the basin. The excellent agreement in both crustal thickness and stretching factors between the two methods is shown in Figs 23 and 24. Fig. 23 shows isostatic crustal reconstructions for mid-Jurassic and pre-Permian times. Superimposed on the mid-Jurassic model are the best-fit pre-stretching crustal thicknesses obtained from the subsidence data (see Fig. 21), shown by diamonds.

Fig. 24 illustrates post-mid-Jurassic stretching factors determined by the two methods, plotted to show variation across the width of the basin. A maximum post-mid-Jurassic β of about 1.6 occurs across the Central Graben itself. Extension west of the Graben is small, but east of the Graben margin a region of post-mid-Jurassic extension (β of approximately 1.2) extends for 100–150 km towards Norway. Also shown in Fig. 24 are total stretching factors since pre-Permian times, estimated from the reconstructed crustal profiles only. Uncertainties in these post-Permian βs are large and reach a maximum in the Central Graben (Table 4); in any case, the assumption that extension was in the plane of the seismic section was probably not realistic for the stretching which created the Permo–Trias basin. This stage

of the reconstruction is discussed elsewhere (Barton & Matthews 1984). Both methods imply a total increase in basin width of about 70 km since the early Jurassic, and the reconstructed crustal model suggests that the total post-Palaeozoic extension is well over 100 km.

6 Conclusions

(1) The post-Triassic North Sea basin was created by a 60 Myr period of lithospheric extension from mid-Jurassic to early Cretaceous times, followed by thermal subsidence to the present day.

(2) During this period of extension the amount of stretching varied across the width of the basin, but reached a maximum β-value of about 1.6 beneath the Central Graben. The basin width appears to have increased by about 70 km during this extensional phase.

(3) Comparison of results from the crustal thickness and subsidence studies show that the mid-Jurassic stretching event occurred on crust already slightly thinned beneath the Central Graben.

(4) The present-day pre-Zechstein crust is best represented as a zone of continuous variation in both seismic velocity and thickness.

(5) Reconstruction of the pre-Permian crustal profile suggests that residual variations in crustal thickness may have been inherited from the Caledonian orogeny, and that over 100 km of extension may have occurred since the Palaeozoic.

(6) Modelling of the observed gravity field indicated that the elastic thickness of the lithosphere of the North Sea is less than 5 km.

Acknowledgments

We thank Drum Matthews and Dan McKenzie for their help and inspiration. Representatives of Amoco, BP, Britoil, Conoco and Shell oil companies and the BGS generously allowed access to velocity data, well logs, and samples. We also thank Peter Ziegler and John Sclater for information and stimulating discussion. The problems of carrying out the seismic work at sea were minimized by the efficiency and cooperation of the officers and crew of *RRS John Murray*. This work was supported by NERC (studentships, ship time, and grant GR3/3932). Cambridge Earth Sciences contribution number 440.

References

Anonymous, 1964. Geological Society Phanerozoic time scale, *Q. Jl geol. Soc. Lond.*, **120**, 260–262.

Bally, A. W., 1982. Musings over sedimentary basin evolution, *Phil. Trans. R. Soc. A*, **305**, 325–336.

Bamford, D., Nunn, K., Prodehl, C. & Jacob, B., 1978. LISPB – IV. Crustal structure of northern Britain, *Geophys. J. R. astr. Soc.*, **54**, 43–60.

Bandy, O. L., 1954. Distribution of some shallow water foraminifera in the Gulf of Mexico, *Prof. Pap. U.S. geol. Surv. 254-F*, 125–141.

Bandy, O. L., 1956. Ecology of foraminifera in northeastern Gulf of Mexico, *Prof. Pap. U.S. geol. Surv. 724-B*, 179–204.

Barton, P. J. & Matthews, D. H., 1984. Deep structure and geology of the North Sea region, *Annls Geophys.*, **6**, in press.

Barton, P. & Wood, R., 1983. Crustal thinning and subsidence in the North Sea; reply to matters arising by P. A. Ziegler, *Nature*, **304**, 561.

Beaumont, C., Keen, C. E. & Boutilier, R., 1982. Foreland and rift margin sedimentary basins, *Phil. Trans. R. Soc. A*, **305**, 295–318.

Berggren, W. A., 1969. Cenozoic chronostratigraphy, planktonic foraminiferal zonation and the radiometric time scale, *Nature*, **224**, 1073.

Bond, G., 1978. Speculations on real sea level changes and motions of continents at selected times in the Cretaceous and Tertiary periods, *Geology*, **6**, 247–250.

Bott, M. H. P., 1976. Formation of sedimentary basins of graben type by extension of continental crust, *Tectonophys.*, **36**, 77–86.

Brennecke, J., Lelgemann, D., Torge, W. & Wenzel, H.-G. (eds), 1982. Validation of *Seasat-1* altimetry using ground truth in the North Sea region, *Reihe B: Angewandte Geodasie Heft Nr 263 Mitteilung Nr 166* des Instituts für Angewandte Geodasie.

Cassell, B. R., 1982. A method for calculating synthetic seismograms in laterally varying media, *Geophys. J. R. astr. Soc.*, **69**, 339–353.

Cassell, B. R., Mykkeltveit, S., Kanestrøm, R. & Husebye, E. S., 1983. A North Sea – Southern Norway seismic crustal profile, *Geophys. J. R. astr. Soc.*, **72**, 733–753.

Červený, V. & Ravindra, R., 1971. *Theory of Seismic Head Waves*, University of Toronto Press, Ontario.

Christie, P. A. F., 1979. The crust and upper mantle beneath the North Sea basin, *PhD thesis*, University of Cambridge.

Christie, P. A. F., 1982. Interpretation of refraction experiments in the North Sea, *Phil. Trans. R. Soc. A*, **305**, 101–111.

Christie, P. A. F. & Sclater, J. G., 1980. An extensional origin for the Buchan and Witchground Graben in the North Sea, *Nature*, **283**, 729–732.

Cochran, J. R., 1982. The magnetic quiet zone in the eastern Gulf of Aden: implications for the early development of the continental margin, *Geophys. J. R. astr. Soc.*, **68**, 171–201.

Collette, B. J., 1960. The gravity field of the North Sea, in *Gravity Expeditions 1948–1958*, **5**, 47–96, ed. Bruins, G. J., Netherlands Geodetic Commission, Delft.

Collette, B. J., Laagay, R. A., Ritzema, A. R. & Schouten, J. A., 1970. Seismic investigations in the North Sea III–VII, *Geophys. J. R. astr. Soc.*, **19**, 183–199.

Day, G. A., Cooper, B. A., Andersen, C., Burgers, W. F. J., Rønnevik, H. C. & Schoneich, H., 1981. Regional seismic structure maps of the North Sea, in *The Petroleum Geology of the Continental Shelf of North-west Europe*, pp. 76–84, eds Illing, L. V. & Hobson, G. D., Heyden, London.

Deegan, C. E. & Brown, S., 1981. Jurassic, in *Introduction to the Petroleum Geology of the North Sea*, JAPEC course notes.

Deegan, C. E. & Scull, B. J., 1977. A standard lithostratigraphic nomenclature for the central and northern North Sea, *Rep. Inst. geol. Sci. 77/25, NPD Bull. 1*, HMSO, London.

Donato, J. A. & Tully, M. C., 1981. A regional interpretation of North Sea Gravity Data, in *The Petroleum Geology of the Continental Shelf of North-west Europe*, pp. 65–75, eds Illing, L. V. & Hobson, G. D., Heyden, London.

Ewing, J. I., 1963. Elementary theory of seismic refraction and reflection measurements, in *The Sea*, **3**, 3–17, ed. Hill, M. N., Wiley, New York.

Foucher, J. P., Le Pichon, X. & Sibuet, J. C., 1982. The ocean-continent transition in the uniform lithospheric stretching model: role of partial melting in the mantle, *Phil. Trans. R. Soc. A*, **305**, 27–43.

Frost, R. T. C., Fitch, F. J. & Miller, J. A., 1981. The age and nature of the crystalline basement of the North Sea Basin, in *The Petroleum Geology of North-west Europe*, pp. 43–57, eds Illing, L. V. & Hobson, G. D., Heyden London.

Garland, G. D., 1979. *Introduction to Geophysics (mantle, core and crust)*, W. B. Saunders, Philadelphia.

Haig, D. W., 1979. Global distribution patterns for mid-Cretaceous foraminiferids, *J. foramaminer. Res.*, **9**, 29–40.

Hancock, J. M., 1981. Cretaceous, in *Introduction to the Petroleum Geology of the North Sea*, JAPEC course notes.

Harland, W. B., Cox, A. V., Llewellyn, P. B., Pickton, C. A., Smith, A. G. & Walters, R., 1982. *A Geologic Time Scale*, Cambridge University Press.

Heelan, P. A., 1953. On the theory of head waves, *Geophysics*, **18**, 871–893.

Illing, L. V. & Hobson, G. D. (eds), 1981. *The Petroleum Geology of the Continental Shelf of North-West Europe*, Heyden, London.

Jackson, J. A., Gagnepain, J., Houseman, G., King, G., Papdimitrious, P., Soufleris, C. & Vinewc, J., 1982. Seismicity, normal faulting and the geomorphological development of the Gulf of Corinth (Greece): the Corinth earthquakes of February & March 1981, *Earth planet. Sci. Lett.*, **57**, 377–397.

Jackson, J. & McKenzie, D., 1983. The geometrical evolution of normal fault systems, *J. struct. Geol.*, **5**(5), 471–482.

Jarvis, G. T. & McKenzie, D. P., 1980. Sedimentary basin formation with finite extension rates, *Earth planet. Sci. Lett.*, **48**, 42–52.

Jenkins, D. G. & Murray, J. W., 1981. *Stratigraphical Atlas of Fossil Foraminifera*, Ellis Horwood, Chichester.

Keen, C. E., Beaumont, C. & Boutilier, R., 1981. A summary of thermo-mechanical model result for the

evolution of continental margins based on three rifting processes, *Hedberg Res. Conf. Am. Ass. Petrol. Geol.*, Galveston.

Le Pichon, X. & Sibuet, J. C., 1981. Passive margins – a model of formation, *J. geophys. Res.*, **86**(B5), 3708–3720.

Ludwig, J. W., Nafe, J. W. & Drake, C. L., 1970. Seismic refraction, in *The Sea*, **4**, 53–84, ed. Maxwell, A. E., Wiley, New York.

McKenzie, D. P., 1978. Some remarks on the development of sedimentary basins, *Earth planet. Sci. Lett.*, **40**, 25–32.

McKenzie, D. P. & Bowin, C., 1976. The relationship between bathymetry and gravity in the Atlantic Ocean, *J. geophys. Res.*, **81**(11), 1903–1915.

Mackenzie, A. S. & McKenzie, D. P., 1983. Isomerization and aromatization of hydrocarbons in sedimentary basins formed by extension, *Geol. Mag.*, **120**(5), 417–470.

Montadert, L., Roberts, D. G., De Charpal, O. & Guennoc, P., 1979. Rifting and subsidence of the Bay of Biscay, *Init. Rep. Deep Sea drill. Proj.*, **48**, 1025–1060.

Murray, J. W., 1971. *An Atlas of British Recent Foraminiferids*, Heineman, London.

Murray, J. W., 1973. *Distribution and Ecology of Living Benthic Foraminiferids*, Heineman, London.

O'Brien, P. N. S. & Lucas, A. L., 1971. Velocity dispersion of seismic waves, *Geophys. Prospect.*, **19**, 1–26.

Parker, F. L., 1948. Foraminifera of the continental slope from the Gulf of Maine to Maryland, *Bull. Harvard Col. Mus. Comp. Zool.*, **100**(2), 213–241.

Parker, F. L., 1954. Distribution of the foraminifera in the northeastern Gulf of Mexico, *Bull. Harvard Col. Mus. Comp. Zool.*, **111**(10), 453–588.

Pflum, C. E. & Frerichs, W. E., 1976. Gulf of Mexico deep water foraminifera, in *Spec. Publ. Cushman Found. foraminifer. Res.*, **14**, ed. Scliter, W. V.

Phleger, F. B., 1951. Foraminifera distribution, in *Ecology of foraminifera, northwest Gulf of Mexico, Mem. geol. Soc. Am.*, **46**, 1–88.

Phleger, F. B., 1960. *Ecological Distribution of Recent Foraminifera*, Johns Hopkins Press, Baltimore.

Pitman, W. C., 1978. Relationships between eustacy and stratigraphic sequences of passive margins, *Bull. geol. Soc. Am.*, **89**, 1389–1403.

Poag, C. W., Harley, J. & Todd, R., 1980. Distribution of modern benthic foraminifera on the New Jersey outer continental shelf, *Mar. Micropaleontol.*, **5**, 43–69.

Proffett, J. M., 1977. Cenozoic geology of the Yerrington district, Nevada and implications for the nature and origin of Basin and Range faulting, *Bull. geol. Soc. Am.*, **88**, 247–266.

Purdy, G. M., 1982. The variability in seismic structure of layer 2 near the East Pacific Rise at 12°N, *J. geophys. Res.*, **87**, 8403–8416.

Rochaw, K. A., 1981. Seismic stratigraphy of the North Sea Palaeocene deposits, in *The Petroleum Geology of the Continental Shelf of North-west Europe*, pp. 255–266, eds Iling, L. V. & Hobson, G. D., Heyden, London.

Royden, L. & Keen, C. E., 1980. Rifting processes and thermal evolution of the continental margin of Eastern Canada determined from subsidence curves, *Earth planet. Sci. Lett.*, **51**, 343–361.

Royden, L., Sclater, J. G. & Von Hertzen, R. P., 1980. Continental margin subsidence and heat flow: important parameters in formation of petroleum hydrocarbons, *Bull. Am. Ass. Petrol. Geol.*, **64**, 173–187.

Ruby, W. W. & Hubbert, M. K., 1960. Role of the fluid pressure in mechanics overthrust faulting II, Overthrust belt in geosynclinal area of western Wyoming in light of fluid pressure hypothesis, *Bull. geol. Soc. Am.*, **60**, 167–205.

Schlanger, S. O. & Jenkyns, H. C., 1976. Cretaceous oceanic anoxic events – causes and consequences, *Geologie Mijnb.*, **55**(3–4), 179–184.

Sclater, J. G. & Christie, P. A. F., 1980. Continental stretching: an explanation of the post Mid-Cretaceous subsidence of the Central North Sea basin, *J. geophys. Res.*, **85**(b7), 3711–3739.

Scliter, W. V. & Baker, R. A., 1972. Cretaceous bathymetric distribution of benthonic foraminiferas, *J. foraminer. Res.*, **2**(4), 167–183.

Sleep, N. H., 1971. Thermal effects of the formation of Atlantic continental margins by continental break-up, *Geophys. J. R. astr. Soc.*, **24**, 325.

Smith, W. A. & Christie, P. A. F., 1977. A pull-up shallow water seismometer, *Mar. geophys. Res.*, **3**, 235–250.

Smythe, D. K., Skuce, A. G. & Donato, J. A., 1980. Geological objections to an extensional origin for the Buchan & Witchground Graben in the North Sea, *Nature*, **287**, 467.

Solli, M., 1976. En seismisk skorpeudersokelse Norges-Shetland, *MSc thesis*, University of Bergen.

Sørnes, A., 1971. Seismic refraction experiments from Norway to Scotland, *PhD thesis,* University of Edinburgh.

Stainsby, S. D. & Worthington, M. H., 1982. Anomalous Q variations in the Central North Sea: estimation from V.S.P. data (abstract, UKGA-6), *Geophys. J. R. astr. Soc.*, **69,** 282.

Steckler, M. S. & Watts, A. B., 1978. Subsidence of the Atlantic type continental margin off New York, *Earth planet. Sci. Lett.*, **41,** 1–13.

Steckler, M. S. & Watts, A. B., 1981. Subsidence history and tectonic evolution of Atlantic-type continental margins, in *Dynamics of Passive Margins,* Geodynamics Series, Vol. 6, American Geophysical Union.

Sutter, A. A., 1980. Paleogene sediments from the United Kingdom sector of the central North Sea, *PhD thesis,* University of Aberdeen.

Taylor, J. C. M., 1981. Zechstein, in *Introduction to the Petroleum Geology of the North Sea,* JAPEC course notes.

Vail, P. R., Mitchum, R. M. & Thompson, S., 1977. Seismic stratigraphy and global changes of sea level, stratigraphic interpretation of seismic data, *Mem. Am. Ass. Petrol. Geol.*, **26,** 83–97.

Walton, W. R., 1964. Recent foraminiferal ecology and palaeocology, in *Approaches to Palaeoecology,* eds Imbrie, J. & Newell, J., Wiley, New York.

Watts, A. B., Karner, G. D. & Steckler, M. S., 1982. Lithospheric flexure and the evolution of sedimentary basins, *Phil. Trans. R. Soc. A,* **305,** 249–281.

Watts, A. B. & Steckler, M. S., 1979. Subsidence and eustacy at the continental margin of eastern North America, *Am. geophys. Un.*, pp. 218–234, *M. Ewing Series 3.*

Wood, R. J., 1981. The subsidence history of Conoco well 15/30–1, central North Sea, *Earth planet. Sci. Lett.*, **54,** 306–312.

Woodhall, D. & Knox, O'B, 1979. Mesozoic volcanism in the northern North Sea and adjacent areas, *Bull. geol. Surv. G. Br.*, **70,** 34–56.

Woodland, A. W. (ed.), 1975. *Petroleum and the Continental Shelf of North-west Europe,* Applied Science, Barking.

Ziegler, P. A., 1978. North Sea rift and basin development, in *Tectonics and Geophysics of Continental Rifts,* pp. 249–277, eds Ramberg, I. B. & Neumann, E. B.

Ziegler, P. A., 1981. Evolution of sedimentary basins in North-west Europe, in *The Petroleum Geology of the Continental Shelf of North-west Europe,* pp. 3–39, eds Illing, L. V. & Hobson, G. D., Heyden, London.

Ziegler, P. A., 1982a. Faulting and graben formation in western and central Europe, *Phil. Trans. R. Soc. A,* **305,** 113–143.

Ziegler, P. A., 1982b. *Geological Atlas of Western and Central Europe,* Shell Internationale Petroleum Maatschappij, B. V.

Ziegler, P. A., 1983. Crustal thinning and subsidence in the North Sea; matters arising, *Nature,* **304,** 561.

Appendix

The following figures and tables appear on microfiche accompanying this issue of *Geophysical Journal*:

(1) Map of seismic experiment.

(2) Table of seismometer positions, North Sea 1981/82.

(3) Table of shot positions and shot instants.

(4)–(15) Seismograms for shots F2, F4 (450 kg), F7, S1, S6, S7, S8, N1, N2, N3, N4, N5. Each reduced at 8.0 km s^{-1}, low pass filtered at 8 Hz, amplitude scaling as in Table 1.

(16) Table of arrival picks from seismograms, with estimated uncertainties, quality graded 1 (very good) to 4 (very poor).

(17)–(35) Compilation of the well data used in computing the subsidence paths.

(36) Comparison of observed and predicted subsidence for the 19 wells assuming earlier stretching event.

(37) Comparison of observed and predicted subsidence assuming uniform initial crustal thickness of 31.2 km.

(38) Comparison between local and flexural (regional) compensation to loading for four wells from the Central Graben.

(39) (a) Well subsidence corrected for compaction. Upper line, before correction, lower line, after correction. (b) Porosity–depth relationships used in decompaction, from Sclater & Christie (1980).

(40) Summary of material used to study each well.